Bachelor's thesis

Drell-Yan Process in the Standard Model and Beyond

Submitted by

Alexander Feike

September 6, 2021

First examiner
Priv.-Doz. Dr. Karol Kovařík

Second examiner
Prof. Dr. Michael Klasen

Westfälische Wilhelms-Universität Münster
Institute for Theoretical Physics
Working Group Klasen

Contents

1. Introduction

Since the first deep inelastic scattering experiments, so the high-energy lepton-hadron scattering, like electron-proton collisions, we learned about the hadronic substructure consisting of quarks, antiquarks and gluons. This concept of a partonic structure may be restored in a hadron-hadron collision, as Drell and Yan suggested in the early 1970s[1]. Following this idea, the Drell-Yan process predicts, for example, the dimuon production by a quark-antiquark annihilation. Today, this is one of the central processes in high-energy particle physics, since it allows to study various phenomena.

In this thesis, we examine the Drell-Yan process with the specific focus on its meaning for Standard Model (SM) propagator particles and Beyond Standard Model (BSM) theories. In section 2 we start with the invariant amplitude and cross section calculations for the explicit subprocess $q\bar{q} \to \gamma/Z^0 \to l^+l^-$ and proceed to the parenting process cross section. Afterwards, we focus on the numerical computation with parton distribution functions (PDFs) in section 3. After discussing some basic properties of the PDFs, we visualize the cross section course and examine the effect of the different propagators. In the last section we handle with the expansion of the SM in the Sequential Standard Model (SSM). It predicts heavier gauge bosons, called Z' and W', which are apart from their masses and widths identical to their SM equivalents. If they exist, they exhibit an influence on the already described cross section, which we will illustrate and explain.

We presume the reader to have a basic knowledge of quantum electrodynamics (QED) because since it is a rather wide field, no explicit background explanations will be given. Only the Feynman rules and some properties and relations of gamma matrices and their traces will be specified in Appendix A.

The conventions in this thesis orientate on the ones used in most of the publications and QED books like [2]. Especially important for the understanding is that we use natural units, so we set the two fundamental constants, the speed of light and the Planck constant, to $c = \hbar = 1$, throughout the whole text. Only when we actually visualize the cross sections and compare them to experimental results, we need to transfer them back to SI units, which will be pointed out explicitly. Furthermore, to separate four- and three-momenta, we denote this by providing a vector arrow over the latter.

2. Theoretics of the Drell-Yan Process

The Drell-Yan process describes the lepton pair production in hadron-hadron collisions and was first suggested by Sidney D. Drell and Tung-Mow Yan[1]. It occurs when a quark and an antiquark of the two hadrons interact, creating a photon or one of the intermediate vector bosons Z^0, W^+ or W^- which decay into a lepton pair. Because the photon and the Z-boson do not carry any charge, their particular partonic subprocesses are given by $q\bar{q} \to \gamma/Z^0 \to l^+l^-$. Since they yield an equivalent process, which is shown in Fig. 1a in lowest order, we have to consider them together in the further derivations.

The W-bosons carry charge and therefore the interacting particles have to be different. Considering the conservation of the lepton family number, the final products have to be a lepton and its related neutrino. Hence a possible process would be $u\bar{d} \to W^+ \to e^+\nu_e$ or $d\bar{u} \to W^- \to e^-\bar{\nu_e}$ where u and d denotes the up- and down-quark. Note that the charged current may occur between two different quark families as well. This is because of the assumption that the W-boson couples to quark states which are rotated with the Cabibbo angle. Nevertheless, transitions like $u\bar{s} \to W^+ \to \mu^+\nu_\mu$ are possible but widely suppressed[2]. The lowest order feynman diagram with a W^+-boson propagator is shown in Fig. 1b.

The calculation of the hadronic cross section σ requires weighting the partonic cross section $\hat{\sigma}$ with the PDFs, which give the probability to find a specific quark in the hadron and will be discussed in detail later. In the following sections, we will therefore concentrate on the subprocess. Since the comparison with experimental data at the end of this thesis focuses on Drell-Yan production with an uncharged propagator, the specific calculations will adopt this focus. The basic idea of how to handle the process with a charged current will be stated, but neither explicit derivations are made nor results discussed.

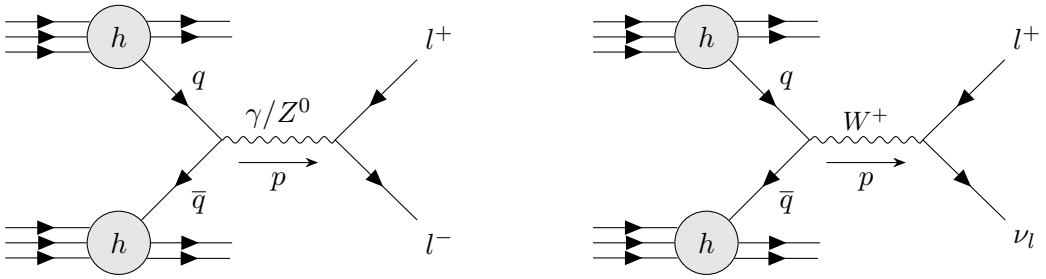

Figure 1: Shown are the lowest order Feynman diagrams of the Drell-Yan process with an uncharged photon or a Z-boson propagator on the left and a charged W^+-boson propagator on the right. For the latter, quark and antiquark may be $u/c/t$ and $\overline{d}/\overline{s}/\overline{b}$ respectively. The equivalent diagram for the W^--boson is not shown but can be obtained by switching the quark and antiquark flavors and the lepton and neutrino with its antiparticles.

2.1. Kinematics

Examining hadronic collisions, it is crucial to distinguish between the hadronic and the partonic centre-of-mass system (CMS). As already mentioned before, the production of lepton pairs in the Drell-Yan process underlies a parton interaction and therefore we will calculate the cross section of the $q\bar{q} \to l^+l^-$ subprocess first. We assign the four-momenta and the corresponding energies p_1, p_2, E_{q_1} and E_{q_2} to the incoming quarks and k_1, k_2, E_{l_1} and E_{l_2} to the outgoing leptons respectively. Due to the conservation of momentum, the propagator momentum is given by the sum $p = p_1 + p_2 = k_1 + k_2$. Furthermore, θ^* describes the scattering angle between $\vec{p}_1$ and $\vec{k}_1$ in the CMS and since we can choose $\vec{p}_1 = |\vec{p}_1|\vec{e}_z$ it is the polar angle. We will only consider high energy collisions so that the particle masses will be neglected from now on. The directions of the momenta in the partonic subsystem are visualized in Fig. 2.

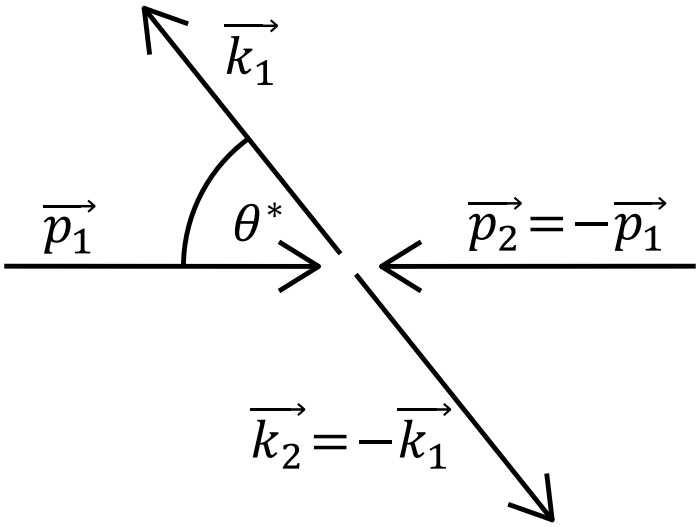

Figure 2: Pictured are the three-momenta and there directions of the $q\bar{q} \to l^+l^-$ interaction in the partonic CMS.

The absolute values of the three-momenta in the CMS are equal and as we neglect the masses, it is clear to see that all four particle energies can be expressed with the centre-of-mass energy $\sqrt{\hat{s}}$ of the partonic system:

$$E_{q_1} = E_{q_2} = E_{l_1} = E_{l_2} = \frac{\sqrt{\hat{s}}}{2}. \tag{2.1}$$

We will use the convention that that variables with a hat describe the partonic system only. Now we may describe four-momenta scalar products with just two variables, the centre-of-mass energy and the scattering angle. For example

$$\hat{s} = (p_1 + p_2)^2 = p_1^2 + p_2^2 + 2p_1 \cdot p_2 \approx 2p_1 \cdot p_2. \tag{2.2}$$

In a similar way, one may also derive

$$p_1 \cdot p_2 = k_1 \cdot k_2 = \frac{p^2}{2} = \frac{\hat{s}}{2} \tag{2.3}$$

$$p_1 \cdot k_1 = p_2 \cdot k_2 = \frac{\hat{s}}{4}(1 - \cos\theta^*) \tag{2.4}$$

$$p_1 \cdot k_2 = p_2 \cdot k_1 = \frac{\hat{s}}{4}(1 + \cos\theta^*) \tag{2.5}$$

$$p \cdot p_1 = p \cdot p_2 = p \cdot k_1 = p \cdot k_2 = \frac{p^2}{2} = \frac{\hat{s}}{2}. \tag{2.6}$$

2.2. Invariant Amplitudes

We may write the differential cross section $d\sigma$ in the general form

$$\mathrm{d}\sigma = \frac{|\mathfrak{M}|^2}{F}\mathrm{d}PS_n \tag{2.7}$$

with the initial flux F, the Lorentz invariant phase space element for an n-particle final state dPS_n and the invariant amplitude $\mathfrak{M}$[2]. Considering the subprocess shown in Fig. 3, there are two different propagators possible, giving us the invariant amplitude as the sum of both $\mathfrak{M} = \mathfrak{M}_\gamma + \mathfrak{M}_Z$. We assign $\mathfrak{M}_\gamma$ to the photon and $\mathfrak{M}_Z$ to the Z-boson propagator. This yields

$$|\mathfrak{M}^2| = |\mathfrak{M}_\gamma^2| + |\mathfrak{M}_Z^2| + 2\,\mathrm{Re}\Big\{\mathfrak{M}_\gamma \mathfrak{M}_Z^\dagger\Big\} \tag{2.8}$$

which we now want to derive step by step with the Feynman rules given in section A.1.

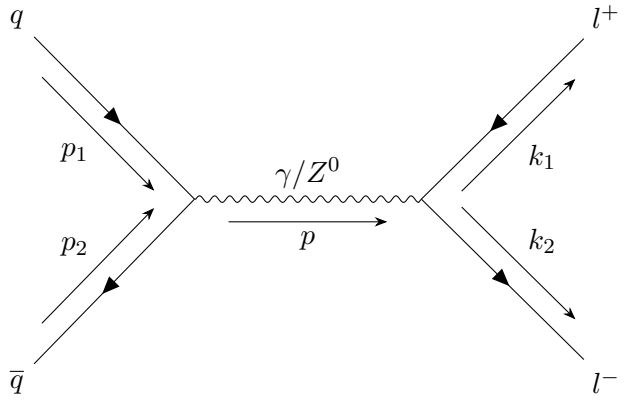

Figure 3: Shown is the Feynman diagram of the subprocess with an uncharged propagator.

2.2.1. Photon Propagator

The invariant amplitude, its adjoint and the square of the absolute value for the photon propagator are

$$-i\mathfrak{M}_\gamma = \bar{v}(p_2) i e_q \gamma^\mu u(p_1) \quad \left(-\frac{i g_{\mu\nu}}{p^2}\right) \quad \bar{u}(k_1) i e_l \gamma^\nu v(k_2) \tag{2.9}$$

$$= \bar{v}(p_2) i e_q \gamma^\mu u(p_1) \ \left(-\frac{i g_{\mu\nu}}{\hat{s}}\right) \ \bar{u}(k_1) i e_l \gamma^\nu v(k_2) \tag{2.10}$$

$$(-i\mathfrak{M}_\gamma)^\dagger = i\mathfrak{M}_\gamma^\dagger = (-ie_q)\bar{u}(p_1)\gamma^\mu v(p_2) \ \frac{ig_{\mu\nu}}{\hat{s}} \ (-ie_l)\bar{v}(k_2)\gamma^\nu u(k_1) \tag{2.11}$$

$$\implies |\mathfrak{M}_\gamma|^2 = \frac{e_q^2 e_l^2}{\hat{s}^2} \ \bar{v}(p_2)\gamma^\mu u(p_1) \ \bar{u}(k_1)\gamma_\mu v(k_2) \ \bar{u}(p_1)\gamma^\nu v(p_2) \ \bar{v}(k_2)\gamma_\nu u(k_1). \tag{2.12}$$

In the unpolarized cross section we do not seperate between different spin states in the initial and final states. Hence we average over the spins of the incoming particles and sum over the spins of the outgoing particles. Assigning the spins s_1 and s_2 to the incoming quarks and s_3 and s_4 to the outgoing leptons, results in the averaged amplitude

$$\overline{|\mathfrak{M}_\gamma|^2} = \frac{1}{4} \sum_{\substack{s_1,s_2,\\ s_3,s_4}} |\mathfrak{M}_\gamma|^2 =: \frac{e_q^2 e_l^2}{\hat{s}^2} L_{\mathrm{q}}^{\mu\nu} L_{\mu\nu}^{\mathrm{l}}. \tag{2.13}$$

To get the calculations well-arranged, we established the tensors $L_{\mathrm{q}}^{\mu\nu}$ and $L_{\mu\nu}^{\mathrm{l}}$ which are associated to the quark and lepton vertex. Their definition

$$L_{\mathrm{q}}^{\mu\nu} := \frac{1}{2} \sum_{s_1,s_2} \bar{v}(p_2)\gamma^\mu u(p_1) \ \bar{u}(p_1)\gamma^\nu v(p_2) \tag{2.14}$$

$$L_{\mu\nu}^{\mathrm{l}} := \frac{1}{2} \sum_{s_3,s_4} \bar{u}(k_1)\gamma_\mu v(k_2) \ \bar{v}(k_2)\gamma_\nu u(k_1) \tag{2.15}$$

allows to separate the calculations. Writing the tensors as the explicit product of matrices and vectors, taking Latin letters as their indices, also giving the assigned spin explicitly and using the completeness relation Eq. A.1 yields:

$$L_{\mathrm{q}}^{\mu\nu} = \frac{1}{2} \sum_{s_1,s_2} \bar{v}_a^{(s_2)}(p_2)\gamma_{ab}^\mu u_b^{(s_1)}(p_1)\bar{u}_c^{(s_1)}(p_1)\gamma_{cd}^\nu v_d^{(s_2)}(p_2) \tag{2.16}$$

$$= \frac{1}{2} \ \not{p}_{1\,bc}\gamma_{cd}^\nu \ \not{p}_{2\,da}\gamma_{ab}^\mu \tag{2.17}$$

$$= \frac{1}{2} \operatorname{Tr}\Big\{\not{p}_1\gamma^\nu\not{p}_2\gamma^\mu\Big\}. \tag{2.18}$$

Using the trace relation Eq. A.4 one may evaluate the quark vertex tensor

$$L_{\mathrm{q}}^{\mu\nu} = \frac{1}{2} p_{1\eta} p_{2\rho} \ \operatorname{Tr}\{\gamma^\eta\gamma^\nu\gamma^\rho\gamma^\mu\} \tag{2.19}$$

$$= \frac{1}{2} p_{1\eta} p_{2\rho} 4 \left(g^{\eta\nu}g^{\rho\mu} - g^{\eta\rho}g^{\nu\mu} + g^{\eta\mu}g^{\nu\rho}\right) \tag{2.20}$$

$$= 2(p_1^\nu p_2^\mu + p_1^\mu p_2^\nu - p_1 \cdot p_2 g^{\nu\mu}) \tag{2.21}$$

and taking the same steps to evaluate the lepton vertex tensor as well:

$$L_{\mu\nu}^{\mathrm{l}} = \frac{1}{2} \sum_{s_3,s_4} \bar{u}_a^{(s_3)}(k_1)\gamma_{\mu_{ab}} v_b^{(s_4)}(k_2)\bar{v}_c^{(s_4)}(k_2)\gamma_{\nu_{cd}} u_d^{(s_3)}(k_1) \tag{2.22}$$

$$= \frac{1}{2} \operatorname{Tr}\{\not{k}_1\gamma_\mu\not{k}_2\gamma_\nu\} \tag{2.23}$$

$$= 2(k_{1\mu}k_{2\nu} + k_{1\nu}k_{2\mu} - k_1 \cdot k_2 g_{\mu\nu}). \tag{2.24}$$

Now we plug them into Eq. 2.13, carry out the multiplications and simplify the occurring scalar products with the results of the kinematic preparations in section 2.1:

$$\overline{|\mathfrak{M}_\gamma|^2} = 4\frac{e_q^2 e_l^2}{\hat{s}^2}(p_1^\nu p_2^\mu + p_1^\mu p_2^\nu - \frac{\hat{s}}{2}g^{\nu\mu})(k_{1\mu}k_{2\nu} + k_{1\nu}k_{2\mu} - \frac{\hat{s}}{2}g_{\mu\nu}) \tag{2.25}$$

$$\begin{aligned} &= 4\frac{e_q^2 e_l^2}{\hat{s}^2}\left[2(p_1 \cdot k_2)(p_2 \cdot k_1) + 2(p_1 \cdot k_1)(p_2 \cdot k_2)\right. \\ &\qquad \left. -\hat{s}\left[(p_1 \cdot p_2) + (k_1 \cdot k_2)\right] + \hat{s}^2\right] \end{aligned} \tag{2.26}$$

$$= 4\frac{e_q^2 e_l^2}{\hat{s}^2}\left[2\left(\frac{\hat{s}}{4}(1 - \cos\theta^*)\right)^2 + 2\left(\frac{\hat{s}}{4}(1 + \cos\theta^*)\right)^2\right] \tag{2.27}$$

$$= e_q^2 e_l^2 (1 + \cos^2\theta^*). \tag{2.28}$$

Similar to allowing all possible spin configurations which led to an averaging, we cannot separate between the color states of the participating quarks either. Hence, we owe to perform the average of the color combinations. There are $N = 3$ possible color states for the quark and antiquark respectively and therefore we have to make the replacement

$$\overline{|\mathfrak{M}_\gamma|^2} \to \frac{1}{N^2}\sum_{\substack{\text{all color}\\ \text{states}}} \overline{|\mathfrak{M}_\gamma|^2}. \tag{2.29}$$

Since the photon as well as the Z- and W-boson do not carry color, the only option is that the interacting quark and antiquark carry color and the associated anticolor. Taking this into account, the sum in either invariant amplitude produces the factor N. Thus, the final spin and color averaged absolute value of the invariant amplitude results in

$$\overline{|\mathfrak{M}_\gamma|^2} = \frac{1}{N} e_q^2 e_l^2 (1 + \cos^2\theta^*). \tag{2.30}$$

2.2.2. Z-Boson Propagator

Once again, we start of by deriving the invariant amplitude and its adjoint for the Z^0-boson propagator

$$\begin{aligned} -i\mathfrak{M}_Z = \bar{v}(p_2)\left(-i\frac{g}{\cos\theta_W}\gamma^\mu\frac{1}{2}\left(c_V^q - c_A^q\gamma^5\right)\right)u(p_1) \quad &\left(\frac{-i\left(g_{\mu\nu} - \frac{p_\mu p_\nu}{M_z^2}\right)}{(p^2 - M_Z^2) + iM_Z\Gamma_Z}\right) \\ \bar{u}(k_1)\left(-i\frac{g}{\cos\theta_W}\gamma^\nu\frac{1}{2}\left(c_V^l - c_A^l\gamma^5\right)\right)v(k_2) & \end{aligned} \tag{2.31}$$

$$\begin{aligned} = -\frac{g^2}{4\cos^2\theta_W} \quad &\bar{v}(p_2)\gamma^\mu\left(c_V^q - c_A^q\gamma^5\right)u(p_1) \quad (-i)\left(\frac{g_{\mu\nu} - \frac{p_\mu p_\nu}{M_z^2}}{(\hat{s} - M_Z^2) + iM_Z\Gamma_Z}\right) \\ &\bar{u}(k_1)\gamma^\nu\left(c_V^l - c_A^l\gamma^5\right)v(k_2) \end{aligned} \tag{2.32}$$

$$i\mathfrak{M}_Z^\dagger = -\frac{g^2}{4\cos^2\theta_W}\ \bar{u}(p_1)\gamma^\rho\left(c_V^q - c_A^q\gamma^5\right)v(p_2)\ \ i\left(\frac{g_{\rho\eta} - \frac{p_\rho p_\eta}{M_z^2}}{(\hat{s}-M_Z^2) - iM_Z\Gamma_Z}\right) \\ \bar{v}(k_2)\gamma^\eta\left(c_V^l - c_A^l\gamma^5\right)u(k_1) \tag{2.33}$$

with the Feynman rules. Due to the fact that there will be a quite similar problem at the end of this thesis, the further calculations will be carried out in a more general way to cover either. So we treat the Z-boson propagator in $\mathfrak{M}_Z$ and $\mathfrak{M}_Z^\dagger$ as if the allocated bosons have different masses and widths but can be treated in the same way regarding all other properties. Acting with foresight, we call the two bosons Z- and Z'-boson. With this specification we evaluate

$$\begin{aligned}\implies \mathfrak{M}_Z\mathfrak{M}_{Z'}^\dagger = \frac{g^4}{16\cos^4\theta_W}&\frac{\left(g_{\mu\nu} - \frac{p_\mu p_\nu}{M_Z^2}\right)}{(\hat{s}-M_Z^2)+iM_Z\Gamma_Z}\frac{\left(g_{\rho\eta} - \frac{p_\rho p_\eta}{M_{Z'}^2}\right)}{(\hat{s}-M_{Z'}^2)-iM_{Z'}\Gamma_{Z'}} \\ &\bar{v}(p_2)\gamma^\mu\left(c_V^q - c_A^q\gamma^5\right)u(p_1)\bar{u}(k_1)\gamma^\nu\left(c_V^l - c_A^l\gamma^5\right)v(k_2) \\ &\bar{u}(p_1)\gamma^\rho\left(c_V^q - c_A^q\gamma^5\right)v(p_2)\ \ \bar{v}(k_2)\gamma^\eta\left(c_V^l - c_A^l\gamma^5\right)u(k_1).\end{aligned} \tag{2.34}$$

Before going on, some tensors will be introduced to arrange the upcoming steps. For the enumerators of the propagators, $P_{\mu\nu}^Z$ and $P_{\rho\eta}^{Z'}$ will be used. Analogue to the derivation of $\mathfrak{M}_\gamma$ there will be tensors associated to the vertex of the quarks $L_\mathrm{q}^{\mu\rho}$ and leptons $L_\mathrm{l}^{\nu\eta}$ as well. We redefine them as

$$P_{\mu\nu}^Z := \left(g_{\mu\nu} - \frac{p_\mu p_\nu}{M_Z^2}\right) \qquad P_{\rho\eta}^{Z'} := \left(g_{\rho\eta} - \frac{p_\rho p_\eta}{M_{Z'}^2}\right) \tag{2.35}$$

$$L_\mathrm{q}^{\mu\rho} := \frac{1}{2}\sum_{s_1,s_2}\bar{v}(p_2)\gamma^\mu\left(c_V^q - c_A^q\gamma^5\right)u(p_1)\ \ \bar{u}(p_1)\gamma^\rho\left(c_V^q - c_A^q\gamma^5\right)v(p_2) \tag{2.36}$$

$$L_\mathrm{l}^{\nu\eta} := \frac{1}{2}\sum_{s_3,s_4}\bar{u}(k_1)\gamma^\nu\left(c_V^l - c_A^l\gamma^5\right)v(k_2)\ \ \bar{v}(k_2)\gamma^\eta\left(c_V^l - c_A^l\gamma^5\right)u(k_1). \tag{2.37}$$

Plugging these tensors into the formula for the spin averaged invariant amplitude yields

$$\overline{\mathfrak{M}_Z\mathfrak{M}_{Z'}^\dagger} = \frac{g^4}{16\cos^4\theta_W}\ \frac{1}{(\hat{s}-M_Z^2)+iM_Z\Gamma_Z}\ \frac{1}{(\hat{s}-M_{Z'}^2)-iM_{Z'}\Gamma_{Z'}}P_{\mu\nu}^Z P_{\rho\eta}^{Z'}L_\mathrm{q}^{\mu\rho}L_\mathrm{l}^{\nu\eta}. \tag{2.38}$$

Using the completeness relation Eq. A.1 and calculating with the explicit product of matrices and vectors as done before for $\mathfrak{M}_\gamma$ one may describe $L_\mathrm{q}^{\mu\rho}$ and $L_\mathrm{l}^{\nu\eta}$ as traces. We can solve these with the trace relations Eq. A.4 and Eq. A.6 as exemplary shown for $L_\mathrm{q}^{\mu\rho}$:

$$L_\mathrm{q}^{\mu\rho} = \frac{1}{2}\mathrm{Tr}\left[\not{p}_1\gamma^\rho\left(c_V^q - c_A^q\gamma^5\right)\not{p}_2\gamma^\mu\left(c_V^q - c_A^q\gamma^5\right)\right] \tag{2.39}$$

$$= \frac{1}{2}p_{1\sigma}p_{2\chi}\mathrm{Tr}\left[\gamma^\sigma\gamma^\rho\left(c_V^q - c_A^q\gamma^5\right)\gamma^\chi\gamma^\mu\left(c_V^q - c_A^q\gamma^5\right)\right] \tag{2.40}$$

$$\begin{aligned}= \frac{1}{2}p_{1\sigma}p_{2\chi}&\left(\left(c_V^q\right)^2\mathrm{Tr}\left[\gamma^\sigma\gamma^\rho\gamma^\chi\gamma^\mu\right] + \left(c_A^q\right)^2\mathrm{Tr}\left[\gamma^\sigma\gamma^\rho\gamma^5\gamma^\chi\gamma^\mu\gamma^5\right]\right. \\ &\left.-c_V^qc_A^q\left(\mathrm{Tr}\left[\gamma^\sigma\gamma^\rho\gamma^5\gamma^\chi\gamma^\mu\right] + \mathrm{Tr}\left[\gamma^\sigma\gamma^\rho\gamma^\chi\gamma^\mu\gamma^5\right]\right)\right)\end{aligned} \tag{2.41}$$

$$
\begin{aligned}
&= \frac{1}{2}\left((c_V^q)^2 + (c_A^q)^2\right) 4\left(p_1^\rho p_2^\mu + p_1^\mu p_2^\rho - p_1 \cdot p_2 g^{\rho\mu}\right) \\
&\quad + c_V^q c_A^q p_{1\sigma} p_{2\chi} 4i(\epsilon^{\chi\mu\sigma\rho} + \epsilon^{\sigma\rho\chi\mu}) \qquad (2.42)\\
&= 2\left\{\left((c_V^q)^2 + (c_A^q)^2\right)\left(p_1^\rho p_2^\mu + p_1^\mu p_2^\rho - \frac{\hat{s}}{2} g^{\rho\mu}\right) + 2ic_V^q c_A^q p_{1\sigma} p_{2\chi} \epsilon^{\sigma\rho\chi\mu}\right\}. \qquad (2.43)
\end{aligned}
$$

Performing the same steps once again, one will gain an analogue expression for $L_1^{\nu\eta}$. After the multiplication of the propagator tensors, the averaged amplitude is given by

$$
\begin{aligned}
\Longrightarrow \overline{\mathfrak{M}_Z \mathfrak{M}_{Z'}^\dagger} &= \frac{g^4}{4\cos^4\theta_W} \frac{\left(g_{\mu\nu} g_{\rho\eta} + \frac{p_\mu p_\nu p_\rho p_\eta}{M_Z^2 M_{Z'}^2} - g_{\mu\nu}\frac{p_\rho p_\eta}{M_{Z'}^2} - g_{\rho\eta}\frac{p_\mu p_\nu}{M_Z^2}\right)}{\left[(\hat{s} - M_Z^2) + iM_Z\Gamma_Z\right]\left[(\hat{s} - M_{Z'}^2) - iM_{Z'}\Gamma_{Z'}\right]} && (2.44a)\\
&\quad \left\{\left((c_V^q)^2 + (c_A^q)^2\right)\left(p_1^\rho p_2^\mu + p_1^\mu p_2^\rho - \frac{\hat{s}}{2} g^{\rho\mu}\right) + 2ic_V^q c_A^q p_{1\sigma} p_{2\chi} \epsilon^{\sigma\rho\chi\mu}\right\} && (2.44b)\\
&\quad \left\{\left(\left(c_V^l\right)^2 + \left(c_A^l\right)^2\right)\left(k_1^\nu k_2^\eta + k_1^\eta k_2^\nu - \frac{\hat{s}}{2} g^{\nu\eta}\right) + 2ic_V^l c_A^l k_{1\tau} k_{2\beta} \epsilon^{\tau\nu\beta\eta}\right\}. && (2.44c)
\end{aligned}
$$

To arrive at a final form for the spin-averaged amplitude, the next steps will be to perform the multiplication of the propagators with the brackets. Since the calculation will be rather long, we will divide it into parts in which the propagator product will be multiplied with one summand of Eq. 2.44b and Eq. 2.44c each. Beginning with the first summands of each bracket but leaving out the factors dependent on the vector and axial vector couplings yields:

$$
\begin{aligned}
&P_{\mu\nu}^Z P_{\rho\eta}^{Z'} \left(p_1^\rho p_2^\mu + p_1^\mu p_2^\rho - \frac{\hat{s}}{2} g^{\rho\mu}\right)\left(k_1^\nu k_2^\eta + k_1^\eta k_2^\nu - \frac{\hat{s}}{2} g^{\nu\eta}\right) && (2.45)\\
&= 2(p_1 \cdot k_2)(p_2 \cdot k_1) + 2(p_1 \cdot k_1)(p_2 \cdot k_2) - \hat{s}(p_1 \cdot p_2) - \hat{s}(k_1 \cdot k_2) + \hat{s}^2 \\
&\quad + \frac{1}{M_Z^2 M_{Z'}^2}\left[4(p_1 \cdot p)(p_2 \cdot p)(k_1 \cdot p)(k_2 \cdot p) - \hat{s}p^2(p_1 \cdot p)(p_2 \cdot p) - \hat{s}p^2(k_1 \cdot p)\right. \\
&\quad \left.(k_2 \cdot p) + \frac{\hat{s}^2}{4} p^4\right] - \left(\frac{1}{M_Z^2} + \frac{1}{M_{Z'}^2}\right)\Big((p \cdot p_1)(p \cdot k_2)(p_2 \cdot k_1) + 2(p \cdot p_1)(p \cdot k_1) && (2.46)\\
&\quad (p_2 \cdot k_2) + (p \cdot p_2)(p \cdot k_2)(p_1 \cdot k_1) + (p \cdot p_2)(p \cdot k_1)(p_1 \cdot k_2) - \hat{s}(p \cdot p_1)(p \cdot p_2) \\
&\quad - \hat{s}(k_1 \cdot p)(k_2 \cdot p) - \frac{\hat{s}^2}{4} p^2\Big).
\end{aligned}
$$

Plugging in the terms derived in section 2.1 for the four vector scalar product, the terms depending on one of the two Z-boson masses vanish. The remaining part, expressed only in the variables of the centre-of-mass energy and the angle between the incoming quark and outgoing lepton in the CMS, reduces to

$$
= \frac{\hat{s}^2}{4}(1 + \cos^2\theta^*). \qquad (2.47)
$$

Going on with the calculations of Eq. 2.44 we will now examine the multiplication of the propagator tensors with the second summand of Eq. 2.44b and Eq. 2.44c each. The crucial aspect is to consider that the Levi-Civita tensor is totally antisymmetric. Thus the product

of a symmetric term such as $p_\mu p_\nu p_\rho p_\eta$ with $\epsilon^{\sigma\rho\chi\mu}$ vanishes. We get

$$P^Z_{\mu\nu}P^{Z'}_{\rho\eta}\left(-4c_V^q c_A^q c_V^l c_A^l p_{1\sigma}p_{2\chi}k_{1\tau}k_{2\beta}\epsilon^{\sigma\rho\chi\mu}\epsilon^{\nu\eta\beta\tau}\right) \tag{2.48}$$

$$\begin{aligned}&= -4c_V^q c_A^q c_V^l c_A^l p_{1\sigma}p_{2\chi}k_{1\tau}k_{2\beta}\left(g^{\sigma a}g^{\chi b}\epsilon_{\nu\eta ab}\epsilon^{\nu\eta\beta\tau} - \frac{p_\rho p_\eta}{M_{Z'}^2}g^{\rho c}g^{\sigma d}g^{\chi e}\epsilon_{\nu cde}\epsilon^{\nu\eta\beta\tau}\right.\\ &\qquad\left. -\frac{p_\mu p_\nu}{M_Z^2}g^{\mu f}g^{\sigma g}g^{\chi h}\epsilon_{\eta fgh}\epsilon^{\eta\nu\beta\tau}\right).\end{aligned} \tag{2.49}$$

Products of ϵ-symbols with partly the same indices can be simplified into Kronecker symbols by applying the relations shown in section A.2. Using them, one finds a term only depending on scalar products, which again reveals a quite compact solution when described with the known variables $\hat{s}$ and θ^*:

$$\begin{aligned}&= -4c_V^q c_A^q c_V^l c_A^l p_{1\sigma}p_{2\chi}k_{1\tau}k_{2\beta}\left\{2g^{\sigma a}g^{\chi b}\left(\delta_b^\beta\delta_a^\tau - \delta_a^\beta\delta_b^\tau\right) + \frac{p_\rho p_\eta}{M_{Z'}^2}g^{\rho c}g^{\sigma d}g^{\chi e}\right.\\ &\quad\left[\delta_c^\eta\left(\delta_d^\beta\delta_e^\tau - \delta_e^\beta\delta_d^\tau\right) + \delta_d^\eta\left(\delta_e^\beta\delta_c^\tau - \delta_c^\beta\delta_e^\tau\right) + \delta_e^\eta\left(\delta_c^\beta\delta_d^\tau - \delta_d^\beta\delta_c^\tau\right)\right] + \frac{p_\mu p_\nu}{M_Z^2}g^{\mu f}\\ &\quad\left.g^{\sigma g}g^{\chi h}\left[\delta_f^\nu\left(\delta_g^\beta\delta_h^\tau - \delta_h^\beta\delta_g^\tau\right) + \delta_g^\nu\left(\delta_h^\beta\delta_f^\tau - \delta_f^\beta\delta_h^\tau\right) + \delta_h^\nu\left(\delta_f^\beta\delta_g^\tau - \delta_g^\beta\delta_f^\tau\right)\right]\right\}\end{aligned} \tag{2.50}$$

$$\begin{aligned}&= 4c_V^q c_A^q c_V^l c_A^l\left\{2(p_1\cdot k_2)(p_2\cdot k_1) - 2(p_1\cdot k_1)(p_2\cdot k_2) - \left(\frac{1}{M_{Z'}^2} + \frac{1}{M_Z^2}\right)\right.\\ &\quad\left[p^2\Big((p_1\cdot k_2)(p_2\cdot k_1) - (p_2\cdot k_2)(p_1\cdot k_1)\Big) + (p\cdot p_1)\Big((p_2\cdot k_2)(p\cdot k_1)\right.\\ &\qquad\left.\left. - (p\cdot k_2)(p_2\cdot k_1)\Big) + (p\cdot p_2)\Big((p\cdot k_2)(p_1\cdot k_1) - (p\cdot k_1)(p_1\cdot k_2)\Big)\right]\right\}\end{aligned} \tag{2.51}$$

$$= 2c_V^q c_A^q c_V^l c_A^l \hat{s}^2\cos\theta^*. \tag{2.52}$$

Now the only parts left to consider of Eq. 2.44 are the mixed terms, so the product of the propagator tensors with the first summand of Eq. 2.44b and the second of Eq. 2.44c and vice versa. We will start of with the first option and again see that the antisymmetry of the Levi-Civita symbol reduces the term a lot:

$$P^Z_{\mu\nu}P^{Z'}_{\rho\eta}\left((c_V^q)^2 + (c_A^q)^2\right)\left(p_1^\rho p_2^\mu + p_1^\mu p_2^\rho - \frac{\hat{s}}{2}g^{\rho\mu}\right)\ 2ic_V^l c_A^l k_{1\tau}k_{2\beta}\epsilon^{\tau\nu\beta\eta} \tag{2.53}$$

$$\begin{aligned}&= 2i\left((c_V^q)^2 + (c_A^q)^2\right)c_V^l c_A^l k_{1\tau}k_{2\beta}\epsilon^{\tau\nu\beta\eta}\left(p_{1\eta}p_{2\nu} + p_{1\nu}p_{2\eta} - \frac{\hat{s}}{2}g_{\nu\eta} - \frac{1}{M_{Z'}^2}[(p\cdot p_1)\right.\\ &\quad p_\eta p_{2\nu} + (p\cdot p_2)p_\eta p_{1\nu} - \frac{\hat{s}}{2}p_\nu p_\eta] - \frac{1}{M_Z^2}[(p\cdot p_1)p_\nu p_{2\eta} + (p\cdot p_2)p_\nu p_{1\eta} - \frac{\hat{s}}{2}p_\nu p_\eta]\Big)\end{aligned} \tag{2.54}$$

$$\begin{aligned}&= 2i\left((c_V^q)^2 + (c_A^q)^2\right)c_V^l c_A^l k_{1\tau}k_{2\beta}\epsilon^{\tau\nu\beta\eta}\left(-\frac{1}{M_{Z'}^2}[(p\cdot p_1)(k_{1\eta}+k_{2\eta})p_{2\nu} + (p\cdot p_2)\right.\\ &\quad (k_{1\eta}+k_{2\eta})p_{1\nu}] - \frac{1}{M_Z^2}[(p\cdot p_1)(k_{1\nu}+k_{2\nu})p_{2\eta} + (p\cdot p_2)(k_{1\nu}+k_{2\nu})p_{1\eta}]\Big)\end{aligned} \tag{2.55}$$

$$= 0. \tag{2.56}$$

From Eq. 2.54 to Eq. 2.55 the obvious products of symmetric terms with the ϵ-symbol were erased. Furthermore, the momentum of the propagator p was assigned to the sum of the momenta k_1 and k_2 like it is shown in section 2.1. This step reveals hidden symmetric products like $k_{1\tau}k_{1\eta}$ which provide that the whole term vanishes. Analogue to this derivation, the product of the other mixed term of Eq. 2.44 disappears as well. Now all products are calculated and we can plug the solutions into Eq. 2.44 and add the color averaging factor $1/N$:

$$\begin{aligned}\overline{\mathfrak{M}_Z\mathfrak{M}_{Z'}^\dagger} = \frac{1}{N}\frac{g^4}{4\cos^4\theta_W}\frac{1}{\left[(\hat{s}-M_Z^2)+iM_Z\Gamma_Z\right]\left[(\hat{s}-M_{Z'}^2)-iM_{Z'}\Gamma_{Z'}\right]} \\ \left\{\left(\left(c_V^q\right)^2+\left(c_A^q\right)^2\right)\left(\left(c_V^l\right)^2+\left(c_A^l\right)^2\right)\frac{\hat{s}^2}{4}(1+\cos^2\theta^*)+2c_V^qc_A^qc_V^lc_A^l\hat{s}^2\cos\theta^*\right\}.\end{aligned} \tag{2.57}$$

To get the spin-averaged amplitude for the pure Z-boson propagator, we now go back from our general solution for two different masses and widths to the particular case with the same masses and widths resulting in

$$\begin{aligned}\overline{|\mathfrak{M}_Z|^2} = \frac{1}{N}\frac{g^4}{16\cos^4\theta_W}\frac{\hat{s}^2}{(\hat{s}-M_Z^2)^2+M_Z^2\Gamma^2}\left\{\left(\left(c_V^q\right)^2+\left(c_A^q\right)^2\right)\right. \\ \left.\left(\left(c_V^l\right)^2+\left(c_A^l\right)^2\right)(1+\cos^2\theta^*)+8c_V^qc_A^qc_V^lc_A^l\cos\theta^*\right\}.\end{aligned} \tag{2.58}$$

The calculations of the invariant amplitude for a charged $W^\pm$-propagator would be equivalent to the Z-propagator in the main steps since the Feynman rules are quite similar. Therefore, one can gain the result by just setting the vector and axial vector coupling factors to one and replace $\cos\theta_W$ with $\sqrt{2}$. To gain this simple transition between Z- and W-boson we neglect the mixing of the quark flavors with the Cabibbo angle. When looking at the CKM-matrix, the assigned mixing matrix, this may be justified since it is nearly the unit matrix.

2.2.3. Interference Term

The interference term $2\,\mathrm{Re}\left\{\mathfrak{M}_1\mathfrak{M}_2^\dagger\right\}$ is now dependent on the already calculated amplitudes. Therefore, we can carry out the multiplication directly:

$$\begin{aligned}\mathfrak{M}_\gamma\mathfrak{M}_Z^\dagger = \frac{g^2e_qe_l}{4\cos^2\theta_W\,\hat{s}}g_{\mu\nu}\left(\frac{g_{\rho\eta}-\frac{p_\rho p_\eta}{M_z^2}}{(\hat{s}-M_Z^2)-iM_Z\Gamma_Z}\right)\bar{v}(p_2)\gamma^\mu u(p_1)\;\bar{u}(k_1)\gamma^\nu v(k_2) \\ \bar{u}(p_1)\gamma^\rho\left(c_V^q-c_A^q\gamma^5\right)v(p_2)\;\bar{v}(k_2)\gamma^\eta\left(c_V^l-c_A^l\gamma^5\right)u(k_1).\end{aligned} \tag{2.59}$$

With the same methods as before, the spin averaging results in traces which can be calculated with the relations given in section A.2. To shorten the expression we omit the prefactor containing the first part of Eq. 2.59 until the Z-boson propagator and the averaging factor

1/4. This yields the proportionality

$$\overline{\mathfrak{M}_\gamma \mathfrak{M}_Z^\dagger} \propto \mathrm{Tr}\Big\{ \not{p}_1 \gamma^\rho \left(c_V^q - c_A^q \gamma^5 \right) \not{p}_2 \gamma^\mu \Big\} \, \mathrm{Tr}\Big\{ \not{k}_1 \gamma^\nu \not{k}_2 \gamma^\eta \left(c_V^l - c_A^l \gamma^5 \right) \Big\} \tag{2.60}$$

$$= p_{1\sigma} p_{2\chi} \, \mathrm{Tr}\Big\{ \gamma^\sigma \gamma^\rho \gamma^\chi \gamma^\mu \left(c_V^q - c_A^q \gamma^5 \right) \Big\} \, k_{1\beta} k_{2\tau} \, \mathrm{Tr}\Big\{ \gamma^\beta \gamma^\nu \gamma^\tau \gamma^\eta \left(c_V^l - c_A^l \gamma^5 \right) \Big\} \tag{2.61}$$

$$\begin{aligned} &= \left[4 c_V^q \left(p_1^\rho p_2^\mu + p_1^\mu p_2^\rho - (p_1 \cdot p_2) g^{\mu\rho} \right) + i \, 4 c_A^q \, p_{1\sigma} p_{2\chi} \epsilon^{\sigma\rho\chi\mu} \right] \\ &\quad \left[4 c_V^l \left(k_1^\nu k_2^\eta + p_1^\eta p_2^\nu - (k_1 \cdot k_2) g^{\nu\eta} \right) + i \, 4 c_A^l \, k_{1\beta} k_{2\tau} \epsilon^{\beta\nu\tau\eta} \right]. \end{aligned} \tag{2.62}$$

Now, the relevant step is to multiply this with the enumerator of the Z-boson propagator and the metric of the photon propagator. Hence, we start by carrying out the multiplication with the first and second brackets, respectively. Using the whole expression yields:

$$\begin{aligned} \overline{\mathfrak{M}_\gamma \mathfrak{M}_Z^\dagger} = \frac{g^2 e_q e_l}{16 \cos^2\theta_W \, \hat{s}} \frac{1}{(\hat{s} - M_Z^2) - i M_Z \Gamma_Z} 16 \Big\{ & c_V^q \left[p_{1\eta} p_2^\mu + p_1^\mu p_{2\eta} - \frac{\hat{s}}{2} g_\eta{}^\mu - \frac{1}{M_Z^2} \right. \\ & \left. \left(\frac{\hat{s}}{2} p_2^\mu p_\eta + \frac{\hat{s}}{2} p_1^\mu p_\eta - \frac{\hat{s}}{2} p^\mu p_\eta \right) \right] - i c_A^q p_{1\sigma} p_{2\chi} \left(\epsilon_\eta{}^{\sigma\chi\mu} - \frac{p_\rho p_\eta}{M_Z^2} \epsilon^{\rho\sigma\chi\mu} \right) \Big\} \\ & \Big\{ c_V^l \left(k_{1\mu} k_2^\eta + k_1^\eta k_{2\mu} - \frac{\hat{s}}{2} g_\mu{}^\eta \right) - i c_A^l k_{1\beta} k_{2\tau} \epsilon_\mu{}^{\beta\tau\eta} \Big\}. \end{aligned} \tag{2.63}$$

Over again, it is crucial to use that the ϵ-symbol is totally antisymmetric and hence vanishes if multiplied with a symmetric expression. The imaginary part of the first curly braces

$$p_{1\sigma} p_{2\chi} p_\rho p_\eta \epsilon^{\rho\sigma\chi\mu} = 0 \tag{2.64}$$

cancels itself out to some extent. Here, the symmetry is hidden and can be shown explicitly if the propagator momentum is written as the sum of the two initial state momenta. The multiplication of the left over imaginary part of these braces with the real part of the second braces

$$p_{1\sigma} p_{2\chi} \left(k_{1\mu} k_2^\eta + k_1^\eta k_{2\mu} - \frac{\hat{s}}{2} g_\mu{}^\eta \right) \epsilon_\eta{}^{\sigma\chi\mu} = 0 \tag{2.65}$$

vanishes as well. A further reduction can be made when multiplying the real part of the first brackets with the imaginary of the second

$$\left[p_{1\eta} p_2^\mu + p_1^\mu p_{2\eta} - \frac{\hat{s}}{2} g_\eta{}^\mu - \frac{1}{M_Z^2} \left(\frac{\hat{s}}{2} p_2^\mu p_\eta + \frac{\hat{s}}{2} p_1^\mu p_\eta - \frac{\hat{s}}{2} p^\mu p_\eta \right) \right] k_{1\beta} k_{2\tau} \epsilon_\mu{}^{\beta\tau\eta} = 0. \tag{2.66}$$

Here again, one has to rewrite the propagator momentum as the sum of the final state momenta. So the only products left are the multiplication of each the real and imaginary parts in the curly braces of Eq. 2.63. Calculating them step by step, starting with the real

parts and including the scalar products from section 2.1 yields

$$\begin{aligned} c_V^q c_V^l \Big[& 2(p_1\cdot k_2)(p_2\cdot k_1) + 2(p_1\cdot k_1)(p_2\cdot k_2) - \hat{s}(p_1\cdot p_2) \\ & - \frac{1}{M_Z^2}\left(\frac{\hat{s}}{2}(p_2\cdot k_1)(k_2\cdot p) + \frac{\hat{s}}{2}(p_2\cdot k_2)(k_1\cdot p) - \frac{\hat{s}^2}{4}(p_2\cdot p) \right. \\ & \quad + \frac{\hat{s}}{2}(p_1\cdot k_1)(p\cdot k_2) + \frac{\hat{s}}{2}(p_1\cdot k_2)(p\cdot k_1) - \frac{\hat{s}^2}{4}(p_1\cdot p) \\ & \quad \left. - \frac{\hat{s}}{2}(p\cdot k_1)(p\cdot k_2) + \frac{\hat{s}^2}{4}(p\cdot p) \right) \Big] \end{aligned} \tag{2.67}$$

$$= c_V^q c_V^l \frac{\hat{s}^2}{4}(1+\cos^2\theta^*). \tag{2.68}$$

For simplifying the remaining product, we use the ϵ-relation Eq. A.12

$$- c_A^q c_A^l p_{1\sigma} p_{2\chi} k_{1\beta} k_{2\tau} \left(\epsilon_\eta{}^{\mu\chi\tau} \;\; \epsilon^\eta{}_\mu{}^{\beta\tau} \right) \tag{2.69}$$

$$= -2c_A^q c_A^l \left[(k_2\cdot p_2)(p_1\cdot k_1) - (p_1\cdot k_2)(p_2\cdot k_1) \right] \tag{2.70}$$

$$= c_a^q c_A^l \frac{\hat{s}^2}{2}\cos\theta^*. \tag{2.71}$$

Now we merge the prefactor with the multiplication results and add the color averaging factor $1/N$. Finally, we just need to calculate the real part of our invariant amplitude product:

$$\begin{aligned} 2\,\mathrm{Re}\left\{ \overline{\mathfrak{M}_\gamma \mathfrak{M}_Z^\dagger} \right\} = 2\mathrm{Re}\Big\{ & \frac{g^2 e_q e_l}{N\cos^2\theta_W}\frac{1}{\hat{s}}\frac{1}{(\hat{s}-M_Z^2)-iM_Z\Gamma_Z} \\ & \left[c_V^q c_V^l \frac{\hat{s}^2}{4}(1+\cos^2\theta^*) + c_a^q c_A^l \frac{\hat{s}^2}{2}\cos\theta^* \right] \Big\} \end{aligned} \tag{2.72}$$

$$\begin{aligned} = & \frac{g^2 e_q e_l}{N\cos^2\theta_W}\hat{s}\left[\frac{1}{2} c_V^q c_V^l (1+\cos^2\theta^*) + c_a^q c_A^l \cos\theta^* \right] \\ & \mathrm{Re}\left\{ \frac{1}{(\hat{s}-M_Z^2)-iM_Z\Gamma_Z} \right\} \end{aligned} \tag{2.73}$$

$$\begin{aligned} = & \frac{g^2 e_q e_l\,\hat{s}}{N\cos^2\theta_W}\frac{\hat{s}-M_Z^2}{(\hat{s}-M_Z^2)^2+M_Z^2\Gamma_Z^2} \\ & \left[\frac{1}{2} c_V^q c_V^l (1+\cos^2\theta^*) + c_a^q c_A^l \cos\theta^* \right]. \end{aligned} \tag{2.74}$$

We completed the calculations for the total invariant amplitude for the Drell-Yan process with an uncharged propagator, which is given by the sum of the amplitude parts in Eq. 2.30, Eq. 2.58 and Eq. 2.74.

2.3. Partonic Cross Section

As mentioned above, the differential cross section may be written in the general form

$$d\sigma = \frac{|\mathfrak{M}|^2}{F} \mathrm{d}PS_n. \tag{2.75}$$

For a collision in the CMS with two particles in the initial and final states each, so $A + B \to C + D$, one can simplify the invariant phase space element as it is shown in [3]:

$$dPS_2 = \frac{1}{4\pi}\frac{1}{2}\ \lambda^{\frac{1}{2}}\left(1, \frac{m_C^2}{s}, \frac{m_D^2}{s}\right)\frac{\mathrm{d}\cos\theta}{2}\frac{\mathrm{d}\varphi}{2\pi}. \tag{2.76}$$

The angles θ and φ denote the polar and angular angle of the scattering process, s is assigned to the square of the centre-of-mass energy and the λ-function is

$$\lambda(x, y, z) = x^2 + y^2 + z^2 - 2xy - 2xz - 2yz. \tag{2.77}$$

Rewriting the λ-function first and then neglecting the masses yields:

$$\mathrm{d}PS_2 = \frac{1}{(4\pi)^2}\frac{\lambda^{\frac{1}{2}}(s, m_C, m_D)}{2s}\ \mathrm{d}\cos\theta\,\mathrm{d}\varphi = \frac{1}{32\pi^2}\,\mathrm{d}\cos\theta\,\mathrm{d}\varphi. \tag{2.78}$$

The flux[2]

$$F = 4\left((p_A \cdot p_B)^2 - m_A^2 m_B^2\right)^{\frac{1}{2}} \tag{2.79}$$

simplifies as well, when using the characteristics of the considered Drell-Yan process. So neglecting the masses and plugging in the known scalar product from Eq. 2.3 one gets

$$F = 2s. \tag{2.80}$$

Therefore, the differential and total partonic cross section of the Drell-Yan process may be evaluated using

$$\mathrm{d}\hat{\sigma} = \frac{|\mathfrak{M}|^2}{2\hat{s}}\frac{1}{32\pi^2}\ \mathrm{d}\cos\theta^*\ \mathrm{d}\varphi. \tag{2.81}$$

$$\implies \hat{\sigma} = \int_{-1}^{1} \mathrm{d}\cos\theta^* \int_0^{2\pi} \mathrm{d}\varphi\ \frac{|\mathfrak{M}|^2}{64\hat{s}\pi^2} = \int_{-1}^{1} \mathrm{d}\cos\theta^* \frac{|\mathfrak{M}|^2}{32\hat{s}\pi} \tag{2.82}$$

Since the invariant amplitude does not depend on φ, we can directly perform its integration. With this relation, we just need to integrate over the scattering angle θ^* to get the total cross section. We separate this like we separated the invariant amplitudes for the different propagators and substitute the charges using the fine structure constant $\alpha = \frac{e^2}{4\pi}$. The lepton charge equals the elementary charge $e_l = e$ but the quark charge does not. Hence, we rewrite the quark charge in units of the elementary charge $e_q \to e_q\, e$ so that $e_q \in \left\{\pm\frac{1}{3}, \pm\frac{2}{3}\right\}$ from

now on. This yields

$$\hat{\sigma}_\gamma = \frac{1}{N}\frac{4\pi\alpha^2}{3\hat{s}}e_q^2 \tag{2.83}$$

$$\hat{\sigma}_Z = \frac{1}{N}\frac{g^4}{192\pi}\frac{1}{\cos^4\theta_W}\frac{\hat{s}}{(\hat{s}-M_Z^2)^2+M_Z^2\Gamma_Z^2}\left((c_V^q)^2+(c_A^q)^2\right)\left(\left(c_V^l\right)^2+\left(c_A^l\right)^2\right) \tag{2.84}$$

$$\hat{\sigma}_{Z/\gamma} = \frac{1}{N}\frac{g^2\alpha e_q}{6\cos^2\theta_W}\frac{\hat{s}-M_Z^2}{(\hat{s}-M_Z^2)^2+M_Z^2\Gamma_Z^2}c_V^q c_V^l. \tag{2.85}$$

The full partonic cross section consists of the sum of the seperated ones.

2.4. Hadronic Cross Section

Now it is time to figure out how we can transfer our results of the partonic subprocess to get the hadronic cross section. If two hadrons A and B collide in the CMS with a fixed centre-of-mass energy S, the interacting partons do not necessarily collide in their CMS and therefore their collision energy is not fixed. We describe the parton momentum as the fraction $0 \leq x < 1$ of the parent hadron momentum. Hence, with the hadron four-momenta

$$P_A = \begin{pmatrix} E_A \\ 0 \\ 0 \\ p_A \end{pmatrix} \qquad P_B = \begin{pmatrix} E_B \\ 0 \\ 0 \\ p_B \end{pmatrix} \tag{2.86}$$

one may derive the parton four-momenta

$$p_1 = \begin{pmatrix} x_1E_A \\ 0 \\ 0 \\ x_1p_A \end{pmatrix} \qquad p_2 = \begin{pmatrix} x_2E_B \\ 0 \\ 0 \\ x_2p_B \end{pmatrix}. \tag{2.87}$$

The parton distribution function (PDF) $f_i(x, Q^2)$ describes the probability that the parton i carries the momentum fraction x of the hadron. Q^2 is the factorization scale and is normally given by the momentum transfer. Factorization theorems yield that the hadronic cross section factorizes into its subprocesses weighted with the integration of the assigned PDFs[3]. Thus, the hadronic cross section may be calculated with

$$\sigma_{hh\to l^+l^-} = \sum_q \int dx_1 dx_2 \left\{ f_q(x_1, M^2) f_{\bar{q}}(x_2, M^2) + (q \leftrightarrow \bar{q}) \right\} \hat{\sigma}_{q\bar{q}\to l^+l^-}(\hat{s}). \tag{2.88}$$

The factorization scale M is typically the momentum transfer, so here it can be connected to the invariant mass of the lepton pair and accordingly to the centre-of-mass energy $\sqrt{\hat{s}}$ later on. A more common way to express the integration variable is with the scaling variable $\tau = x_1x_2$ and the rapidity of the parton system in the lab frame y_{cm}. Considering a ring collider for example, so the lab frame equals the centre-of-mass frame of the hadron collision,

the energy of the particles is equal and the momentum is just directed in opposite directions. Applying this on Eq. 2.86 and Eq. 2.87, the centre-of-mass energies may be connected

$$S = (P_A + P_B)^2 = \begin{pmatrix} 2E_A \\ 0 \\ 0 \\ 0 \end{pmatrix}^2 = 4E_A \tag{2.89}$$

$$\hat{s} = (p_1 + p_2)^2 = \begin{pmatrix} (x_1 + x_2)E_A \\ 0 \\ 0 \\ (x_1 - x_2)E_A \end{pmatrix}^2 = 4E_A^2 x_1 x_2 = \tau S \tag{2.90}$$

$$\implies \frac{\hat{s}}{S} = \tau. \tag{2.91}$$

Here the masses were already neglected, so that $E_A = p_A$. To get an expression for the parton system rapidity, we first describe the momentum P_{cm} and plug this into the rapidity:

$$P_{cm} = (p_1 + p_2) = \big((x_1 + x_2)E_A, 0, 0, (x_1 - x_2)E_A\big) \tag{2.92}$$

$$\beta_{cm} = \frac{|\vec{P}_{cm}|}{E_A} = \frac{x_1 - x_2}{x_1 + x_2} \tag{2.93}$$

$$\implies y_{cm} = \frac{1}{2}\ln\left(\frac{1+\beta_{cm}}{1-\beta_{cm}}\right) = \frac{1}{2}\ln\left(\frac{x_1}{x_2}\right). \tag{2.94}$$

With these relations, we may express the fractions x as

$$x_{1/2} = \sqrt{\tau} e^{\pm y_{cm}}. \tag{2.95}$$

With these variables, we rewrite the hadronic cross section. We directly use that the particles are approximately massless, so the interval of integration simplifies

$$\begin{aligned} \sigma_{hh\to l^+l^-} = \sum_q \int_0^1 d\tau \int_{\frac{1}{2}\ln\tau}^{-\frac{1}{2}\ln\tau} dy_{cm}\ \hat{\sigma}_{q\bar{q}\to l^+l^-}(\tau S) \\ \Big\{ f_q(\sqrt{\tau}e^{y_{cm}}, M^2) f_{\bar{q}}(\sqrt{\tau}e^{-y_{cm}}, M^2) + (q \leftrightarrow \bar{q}) \Big\}. \end{aligned} \tag{2.96}$$

This expression can only be evaluated numerically and will therefore be part of the next chapter.

3. Numerical and Experimental Evaluation

In this section, we will concentrate on a comparison of the numerical evaluations of the hadronic cross sections with the experimental data. The computation is based on the most recent PDF set CT18nnlo[4], which describes the parton density in protons and antiprotons. Hence, the selected experimental data from Fermilab includes proton-proton and proton-antiproton collisions only. All numeric evaluations will be made with Python 3.9.5 and in particular with the parton package from LHAPDF[5].

3.1. PDF

Revealing the fundamental structure of nucleons is one of the major topics in particle physics, hence parton distributions of hadrons are relevant. They play a central role in the upcoming numerical computations for hadronic cross sections and therefore we want to gain some basic knowledge about them. First, the general idea of PDFs, how they are obtained from experiments and how to use them when calculating cross sections will be given. The explanations, especially regarding the derivation of the PDFs from experiments, will not be exact nor complete but give an overview. For further details, one may consult [6]. Afterwards, some applied parts of the PDFs will be addressed by means of the particular PDF set CT18nnlo.

3.1.1. PDFs in General

As stated before, the PDF $f_i^{(h)}(x)$ yields the probability to find the parton i carrying the momentum fraction x in the hadron h. Right now, it is not possible to get the PDFs from first principle and so they are determined by comparing calculated hadronic cross section predictions with experimental measured data. Data from deep-inelastic scattering, Drell-Yan production, jet and hadron production and top production from high energy experiments are mainly taken into account to cover different areas of transmitted energy Q and momentum fraction x. The PDF itself is assumed to be a function of different parameters which are determined by fitting the function over the data in a procedure called global QCD analysis[6].

There are different constraints which have to be considered while modeling the theoretical PDF. For instance, the momentum conservation implies that all the parton momenta have to sum up to the hadrons momentum

$$\sum_i \int_0^1 x f_i^{(h)}(x) \mathrm{d}x = 1 \tag{3.1}$$

which is sometimes called completeness relation, too. Furthermore, the PDFs have to conserve the structure of the hadrons valence quarks. This yields for the proton for example

$$\int_0^1 \left(f_u^{(P)}(x) - f_{\bar{u}}^{(P)}(x)\right) \mathrm{d}x = 2 \qquad \int_0^1 \left(f_d^{(P)}(x) - f_{\bar{d}}^{(P)}(x)\right) \mathrm{d}x = 1 \tag{3.2}$$

and the same calculation for all other quarks has to give 0[6].

When computing higher order partonic cross section singularities emerge which are fixed by renormalization. As the PDFs have to be renormalized as well, a scale dependence is needed. In this whole thesis, it is always set to the transmitted energy, so $f_i^{(h)}(x, Q^2)$. Note that this scaling variable is unphysical and the hadronic cross sections do not depend on this when calculated with all perturbative orders[6]. We will have a closer look at the PDF scaling of the CT18nnlo set and give a further discussion. In this text, all calculations are done at tree level. Considering that the scaling is unphysical, we add a scaling uncertainty, by calculating the cross sections with the ideal scaling variable Q and moreover with $2Q$ and $1/2\,Q$ to get a scaling uncertainty band.

A general PDF set contains different members, one with the information about the optimum values and the others with the information about the PDF uncertainty. These occur in pairs f^+ and f^- that belong together and give the aberration above and below the best values. To calculate the PDF intrinsic uncertainty of an observable X that depends on the distribution, we use[7]

$$\Delta X = \frac{1}{2}\sqrt{\sum_k \left[X(f_k^+) - X(f_k^-)\right]^2}. \tag{3.3}$$

3.1.2. CT18nnlo

CT18nnlo is a PDF set, which was presented by the multi-institutional collaboration CTEQ. They are worked out by taking data of different processes like deep inelastic scattering or the production of Drell-Yan pairs and fit them with next-to-next-to-leading order calculations[4]. Checking the completeness relation Eq. 3.1 for CT18nnlo, it is striking that the quarks and antiquarks only carry a percentage of approximately 54 % of the protons momentum. Historically, the first experiment that really showed some kind of parton distribution in form of the structure functions is the deep inelastic scattering. Since only the quarks and antiquarks participate in this scattering, the physicists also noticed a similar fraction of the protons momentum was unfound. This marks the start of the research on the field theory of the strong interaction, the quantum chromodynamics (QCD). Later on, the gluon, the quantum of the color field, was found[8]. Adding up the CT18nnlo momenta of the constituents with the gluons, one finds just a small aberration from 100 % which can be explained by inaccuracies from numerical integration.

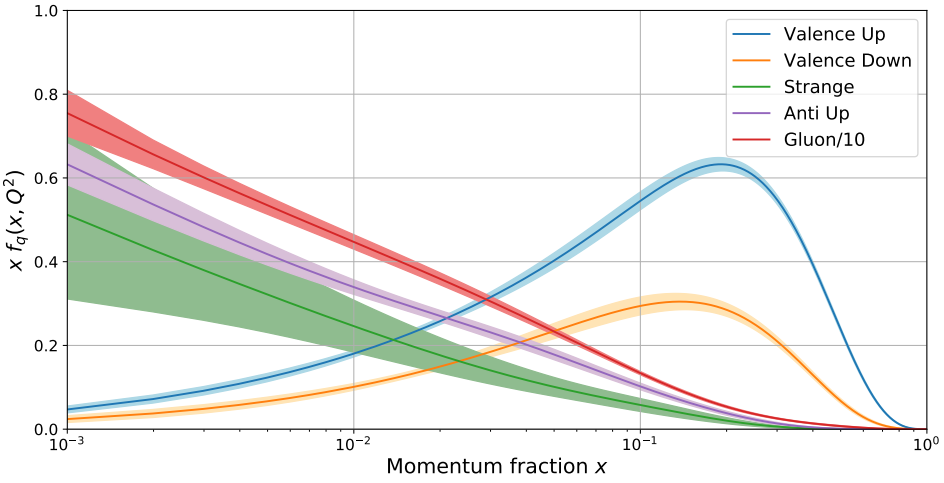

(a) $Q = 10\,\mathrm{GeV}$

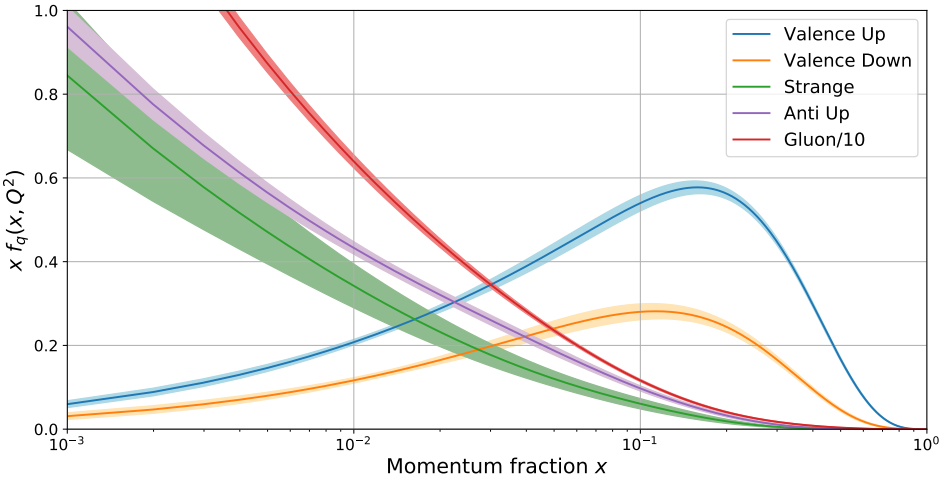

(b) $Q = 100\,\mathrm{GeV}$

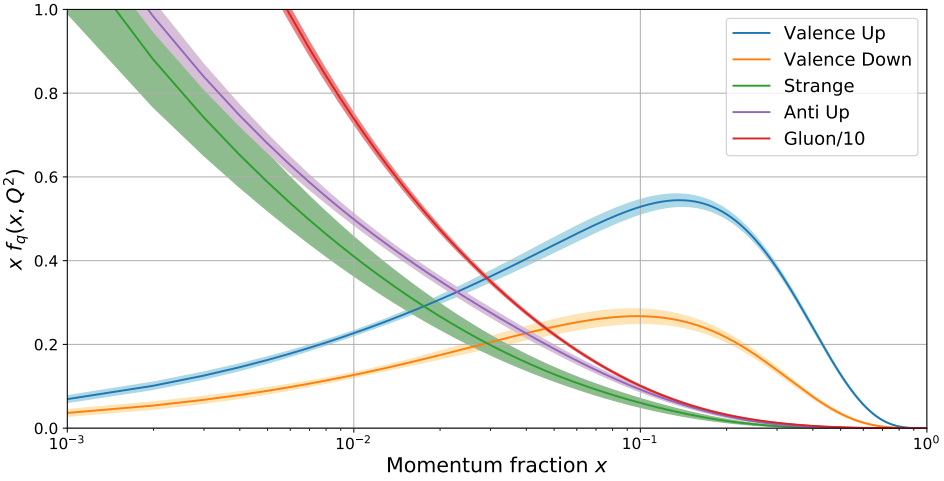

(c) $Q = 1000\,\mathrm{GeV}$

Figure 4: Shown is the distribution $x f_q(x, Q^2)$ of some exemplary quarks, antiquarks and the gluon in the proton at different scaling energies according to CT18nnlo[4]. For clarity, the gluon distribution is multiplied with the factor 1/10.

One may gain a general insight into the parton distribution of the proton when looking at Fig. 4. The exemplary distribution for some quarks, antiquarks and the gluon validates the high momentum fraction of the gluon, which is presented with the factor 1/10. Furthermore, one can see that the valence quarks dominate only for x-values higher than approximately 10^{-1}. For decreasing fractions x the distribution for the sea quarks and gluons increases and decreases for the valence quarks. So the probability to find a sea quark that carries just a small part of the protons momentum is higher than to find one which carries a big part of the momentum.

A further information about PDFs that is gained when comparing the different scaling of the energy plots in Fig. 4. With higher energies, the distributions with small values of x are increasing, while the distributions with high values are decreasing. This means that with higher energy, the momentum is divided in smaller packages. This phenomenon is called scaling violation and we can explain it with the continuous interaction of the quarks in the hadron which leads to a permanent change in the distribution. As we know from QCD, quarks can emit and absorb gluons, while loosing or gaining momentum. Furthermore, the gluon may emit quark-antiquark pairs or further gluons[8].

Thinking of deep inelastic scattering for example, it is clear to see that the resolution of the virtual photon is dependent on its wavelength and therefore increases with $\propto \hbar/\sqrt{Q^2}$. So at lower energies, it is possible that the resolution is not high enough to separate a quark and an emitted gluon. On the other hand, at higher energies one can measure more separate particles and therefore the hadron momentum divides into smaller parts. The change of the PDF with the scaling energies is proportional to the strong coupling constant $\alpha_S(Q^2)$ and can be calculated with the so called DGLAP equations. This means, while gaining information about the distribution functions via experiments, theoretically one only needs the results of the experiments at one energy[8].

3.2. Scaling Behaviour of the Drell-Yan Cross Section

We can easily convert the subprocess cross sections from section 2.3 into a differential cross sections of the hadron collision. The cross section for the production of a lepton pair with the squared invariant mass M^2 may be derived via

$$\frac{\mathrm{d}\hat{\sigma}}{\mathrm{d}M^2} = \hat{\sigma}\ \ \delta\left(\hat{s} - M^2\right). \tag{3.4}$$

The squared centre-of-mass energy may be transformed into the variables used for the hadronic cross section. So taking $\hat{s} = \tau S$ into the delta function, it can be rewritten like

$$\delta\left(\hat{s} - M^2\right) = \delta\left(\tau S - M^2\right) = \frac{1}{S}\,\delta\left(\tau - \frac{M^2}{S}\right) \tag{3.5}$$

where we neglect the absolute value of S because $S \geq 0$. The corresponding differential hardronic cross section is computed by plugging the differential subprocess cross section into Eq. 2.96. Doing this for the photon propagator yields:

$$\begin{aligned}\frac{\mathrm{d}\sigma_\gamma}{\mathrm{d}M^2} = \frac{4\pi\alpha^2}{3NM^2}\sum_q e_q^2 \int_0^1 d\tau \int_{\frac{1}{2}\ln\tau}^{-\frac{1}{2}\ln\tau} dy_{cm}\ \{f_q^{(h)}(\sqrt{\tau}e^{y_{cm}}) f_{\bar{q}}^{(h)}(\sqrt{\tau}e^{-y_{cm}}) \\ + (q \leftrightarrow \bar{q})\}\frac{1}{S}\,\delta\left(\tau - \frac{M^2}{S}\right)\end{aligned} \tag{3.6}$$

$$\begin{aligned}\implies M^4\frac{\mathrm{d}\sigma_\gamma}{\mathrm{d}M^2} = \frac{4\pi\alpha^2}{3N}\tau\sum_q e_q^2 \int_{\frac{1}{2}\ln\tau}^{-\frac{1}{2}\ln\tau} dy_{cm}\ \{f_q^{(h)}(\sqrt{\tau}e^{y_{cm}}) f_{\bar{q}}^{(h)}(\sqrt{\tau}e^{-y_{cm}}) \\ + (q \leftrightarrow \bar{q})\}.\end{aligned} \tag{3.7}$$

$$=: \frac{4\pi\alpha^2}{3N}\tau F(\tau). \tag{3.8}$$

This central result shows that the differential cross section exhibits scaling in the variable τ. Here, this means it is not individually dependent on M^2 and S but on their quotient only and may be seen as the analogous to the Bjorken scaling in deep inealstic scattering. Of course this is only possible while neglecting the already discussed scaling violation from QCD. The Q^2 dependence is especially striking at low x-values.

3.2.1. Experimental and Numerical Data

The photon is massless, while the Z-boson mass is in the GeV-region. Therefore, we would expect the Drell-Yan process to show scaling behaviour at low M^2, so at low energies. To check this result, we want to compare it with experimental measured cross sections. In the following discussion, we use data from the fixed target Fermilab experiment 772. Protons get accelerated and collide with targets of deuterium, carbon, calcium, iron and tungsten at a centre-of-mass energy of $\sqrt{S} = 38.7\,\mathrm{GeV}$[9]. The data is already cleared of the neutron scatterings, so we can treat it like a proton-proton collision. The measurement of the muon pairs is seperated by three different sized mass triggers and the data is transferred to the differential cross section $\frac{d\sigma}{dM}$. The theoretically determined cross section from Eq. 3.7 will thus be expressed with

$$\frac{\mathrm{d}\sigma_\gamma}{\mathrm{d}M} = 2M\frac{\mathrm{d}\sigma_\gamma}{\mathrm{d}M^2}. \tag{3.9}$$

For the numerical evaluation with the parton package, it is important to notice that the intrinsic PDF function is $xf(x)$. So the term

$$\frac{\mathrm{d}\sigma_\gamma}{\mathrm{d}M^2} = \frac{8\pi\alpha^2}{3NM^3}\sum_q e_q^2 \int_{\frac{1}{2}\ln\tau}^{-\frac{1}{2}\ln\tau} \mathrm{d}y_{cm} \\ \{\sqrt{\tau}e^{y_{cm}} f_q(\sqrt{\tau}e^{y_{cm}})\ \ \sqrt{\tau}e^{-y_{cm}} f_{\bar{q}}(\sqrt{\tau}e^{-y_{cm}}) + (q \leftrightarrow \bar{q})\} \tag{3.10}$$

gets finally plugged in the python code. The hadron is not denoted in the superscript anymore because now we only regard proton PDFs. The constants for the numerical evolution

$$c = 299\,792\,458\,\mathrm{m\,s^{-1}} \qquad \hbar = 6.582\,119\,569 \times 10^{-25}\,\mathrm{GeV\,s} \tag{3.11}$$

$$\alpha = 7.297\,352\,569\,3 \times 10^{-3} \tag{3.12}$$

are taken from [10, Reviews > Physical constants]. To gain the cross section dimension m^2, the natural units get transferred back via the factor $(\hbar c)^2$.

There are two different uncertainties that we have to take care of while calculation cross sections with PDFs. The first one is the intrinsic PDF uncertainty which we can transmit to any observable with Eq. 3.3 and the second one results from scaling. In the following discussion the intrinsic PDF uncertainty and the square root of the quadratic addition of both uncertainties will be shown explicitly. They clearly dominate any uncertainties from constants, which therefore will be neglected.

3.2.2. Comparison of Experiment and Numerics

Both the experimental and the numerical results are shown in Fig. 5. Apart from two peaks at around 3 GeV and 10 GeV, the measured and numerical data exhibit the same course. Nearly all points overlap with the uncertainty band and hence confirm that the computed results are a good prediction, although we only use the photon propagator, which was calculated at tree level.

The two peaks can be physically discussed as well. In the experiment, many events are measured, but our data is cleared in a way that we only get the cross section for dilepton production. So in this manner, it is possible to only get the data which fits to our final state. Since it is not possible to know their origin, they may not be produced via the direct $q\overline{q} \to \gamma/Z^0 \to l^+l^-$ process, but for example the quarks got engaged into a bound state before they decay. The course of the peaks suggest, that they are such hadron resonances which deacy into a lepton pair. Compared with the masses of neutral mesons, one finds, for example, the $J/\Psi(1S)$ resonance, which is the most common bound charmonium state. Considering the mass of $m_{J/\Psi} = 3.0969\,\mathrm{GeV}$ and the branching ratio $\frac{\Gamma(J/\Psi\to\mu^+\mu^-)}{\Gamma(J/\Psi)} = 5.961\,\%$[10, Summary Tables > Mesons], indicates that the first peak shows a charmonium resonance

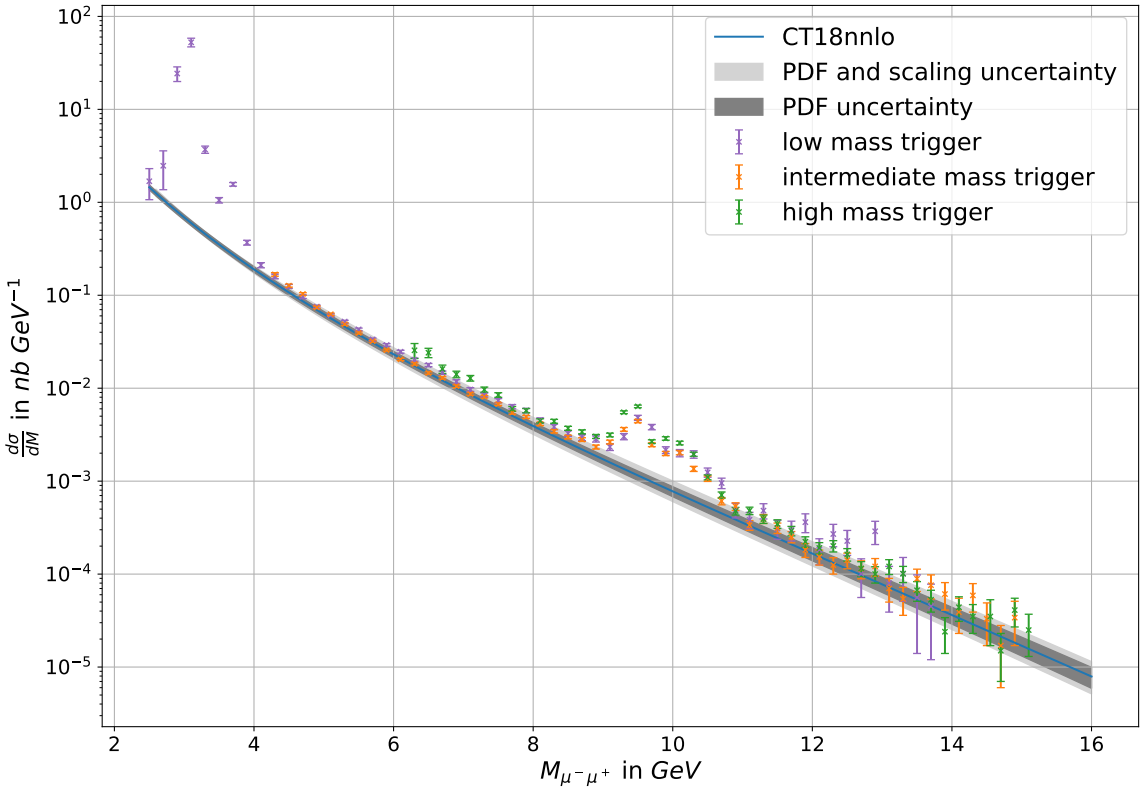

Figure 5: Shown is the experimental data from [9] for the hadronic cross section as well as the calculated prediction for the photon propagator only with CT18nnlo. Note that the y-axis is scaled logarithmic.

like the J/Ψ.

The second peak seems to be an overlay of two different resonances because at least two summits may be be separated. Considering the quark masses, one should especially take bound $b\bar{b}$ states into account, like the Υ meson. For the different energy levels there are, for example, the $\Upsilon(1S)$ particle with $m_{\Upsilon(1S)} = 9.460\,\text{GeV}$, which decays into a muon pair with 2.48 % or the $\Upsilon(3S)$ with $m_{\Upsilon(3S)} = 10.355\,\text{GeV}$ and a decay probability of 2.18 %[10, Summary Tables > Mesons].

Finally, we want to have a look at the uncertainty band which seems to widen up at higher energies. Here, the crucial point is to remember the logarithmic scaled y-axis. Actually the PDF uncertainty decreases at higher energies which is now consistent with the bands shown in Fig. 4. The scaling uncertainty band narrows as well with higher energies.

3.3. Drell-Yan Cross Section with Z- and W-Bosons

The Z-boson cross section and the mixed term cannot be neglected when considering higher momentum transfers. Therefore, we now want to calculate the differential cross section $\mathrm{d}^2\sigma/(\mathrm{d}M\ \mathrm{d}y_{cm|y_{cm}|<1})$ for all terms and compare it to experimental measured data. The

used expression for the differential cross section will be explained in a moment. Afterwards we will give the idea on how to measure the W-boson peak.

3.3.1. Z-Boson

The experimental data originates from proton-antiproton collision in the Collider Detector at Fermilab (CDF) from the 1988-1989 run[11] and the runs in 1992-1993 and 1994-1995[12] at a centre-of-mass energy of $\sqrt{S} = 1.8\,\mathrm{TeV}$. The invariant lepton mass range is $11 \leq M_{l^+l^-} \leq 150\,\mathrm{GeV}$ and $40 \leq M_{l^+l^-} \leq 500\,\mathrm{GeV}$ respectively, where the lepton pairs were assigned into bins. Error bars will show the bin width later on. Only dileptons with a rapidity of $|y_{cm}| < 1$ are taken into consideration and the data is transferred to the differential cross section $\mathrm{d}^2\sigma/(\mathrm{d}M\ \mathrm{d}y_{cm|y_{cm}|<1})$.

The semi correct differential cross section expression which is adopted from the experimental publications is just an abbreviation for

$$\frac{\mathrm{d}^2\sigma}{\mathrm{d}M\ \mathrm{d}y_{cm_{|}y_{cm}|<1}} := \frac{1}{2}\int_{-1}^{1}\frac{\mathrm{d}^2\sigma}{\mathrm{d}M\ \mathrm{d}y_{cm}}\mathrm{d}y_{cm} \tag{3.13}$$

with the factor $1/2$ to account for the two units of rapidity. So with the same steps as before and for a general subprocess cross section $\hat{\sigma}(\hat{s})$ we gain

$$\frac{1}{2}\int_{-1}^{1}\frac{\mathrm{d}^2\sigma}{\mathrm{d}M\ \mathrm{d}y_{cm}}\mathrm{d}y_{cm} = M\frac{\mathrm{d}\sigma}{\mathrm{d}M^2}\int_{-1}^{1}\frac{\mathrm{d}\sigma}{\mathrm{d}y_{cm}}\mathrm{d}y_{cm} \tag{3.14}$$

$$= \frac{M}{S}\sum_q \int_0^1 d\tau \int_{-1}^{1}\mathrm{d}y_{cm}\ \hat{\sigma}(\tau S)\ \delta\left(\tau - \frac{M^2}{S}\right) \left\{f_q^{(P)}(\sqrt{\tau}e^{y_{cm}}, M^2) f_{\bar{q}}^{(\bar{P})}(\sqrt{\tau}e^{-y_{cm}}, M^2) + (q \leftrightarrow \bar{q})\right\} \tag{3.15}$$

$$= \frac{1}{M}\sum_q \hat{\sigma}(M^2)\mathcal{Y} \tag{3.16}$$

$$\text{with:} \qquad \mathcal{Y} := \int_{-1}^{1}\mathrm{d}y_{cm}\left\{\sqrt{\frac{M^2}{S}}e^{y_{cm}}\ f_q^{(P)}\left(\sqrt{\frac{M^2}{S}}e^{y_{cm}}, M^2\right) \sqrt{\frac{M^2}{S}}e^{-y_{cm}} f_{\bar{q}}^{(\bar{P})}\left(\sqrt{\frac{M^2}{S}}e^{-y_{cm}}, M^2\right) + (q \leftrightarrow \bar{q})\right\}. \tag{3.17}$$

Note that the superscripts of the PDFs now explicitly show which hadron is described, a proton or antiproton. We still take the PDF set CT18nnlo for both, but have to be cautious to assign the quark distribution of the proton PDF to the antiquark distribution of the antiproton PDF. For example, the probability to find an up quark in the proton is the same as the probability to find an anti-up in the antiproton for all momentum fractions x.

Moreover, we introduced the variable $\mathcal{Y}$ for the rapidity integration over the PDFs. Considering a particle collider, one gains the rate of events as the product of the cross section and teh luminosity, a factor determined by the collider properties. Here the calculations are independent of any machine parameters but we still may express it as the product of the partonic cross section and a factor which now depends on the hadronic process. Because of the similarity we call this factor $\mathcal{Y}$ a parton luminosity as well[13].

Taking the partonic cross sections from Eq. 2.83, Eq. 2.84 and Eq. 2.85 and plugging them into Eq. 3.16 yields

$$\frac{1}{2}\int_{-1}^{1}\frac{\mathrm{d}^2\sigma_\gamma}{\mathrm{d}M\,\mathrm{d}y_{cm}}\mathrm{d}y_{cm} = \frac{4\pi\alpha^2}{3N}\frac{1}{M^3}\sum_q e_q^2\,\mathcal{Y} \tag{3.18}$$

$$\begin{aligned}\frac{1}{2}\int_{-1}^{1}\frac{\mathrm{d}^2\sigma_{Z^0}}{\mathrm{d}M\,\mathrm{d}y_{cm}}\mathrm{d}y_{cm} = {} & \frac{g^4}{192N\pi\cos^4\theta_W}\,\frac{M}{(M^2-M_Z^2)^2+M_Z^2\Gamma_Z^2} \\ & \left(\left(c_V^l\right)^2+\left(c_A^l\right)^2\right)\sum_q\left((c_V^q)^2+(c_A^q)^2\right)\mathcal{Y}\end{aligned} \tag{3.19}$$

$$\frac{1}{2}\int_{-1}^{1}\frac{\mathrm{d}^2\sigma_{Z^0/\gamma}}{\mathrm{d}M\,\mathrm{d}y_{cm}}\mathrm{d}y_{cm} = \frac{g^2\alpha c_V^l}{6N\cos^2\theta_W}\,\frac{M^2-M_Z^2}{(M^2-M_Z^2)^2+M_Z^2\Gamma_Z^2}\,\frac{1}{M}\,\sum_q e_q c_V^q\,\mathcal{Y} \tag{3.20}$$

which may be added to get the final differential hardronic cross section. The left over constant values are again used without uncertainties and they are taken from [10, Summary Tables > Gauge and Higgs Bosons]:

$$M_Z = 91.1876\,\mathrm{GeV} \qquad \Gamma_Z = 2.4952\,\mathrm{GeV} \tag{3.21}$$

$$\sin^2\theta_W = 0,22337 \qquad g = \frac{\sqrt{4\pi\alpha}}{\sin\theta_W} \tag{3.22}$$

$$c_V^{u/c/t} = 0,266 \qquad c_A^{u/c/t} = 0,519 \tag{3.23}$$

$$c_V^{d/s/b} = -0,38 \qquad c_A^{d/s/b} = -0,527 \tag{3.24}$$

$$c_V^{l} = -0,03783 \qquad c_A^{l} = -0,50123. \tag{3.25}$$

The experimental measured invariant mass of the lepton pair and the final numerical results are shown in Fig. 6. The measured observable already yields a peak at the Z-boson mass, as expected. The numerical computations show a very good agreement, since at least the uncertainty areas of the points overlap with the prediction for the complete dataset. Hence, the cross section calculations at leading order, except for the Breit-Wigner peak, already describe the process well. Furthermore, it is quite clear to see that by measuring the invariant lepton mass, one directly gets the partonic centre-of-mass energy $\sqrt{\hat{s}}$ which also describes the propagator energy due to momentum conservation.

Considering only the pure photon propagator cross section and the measured data, we

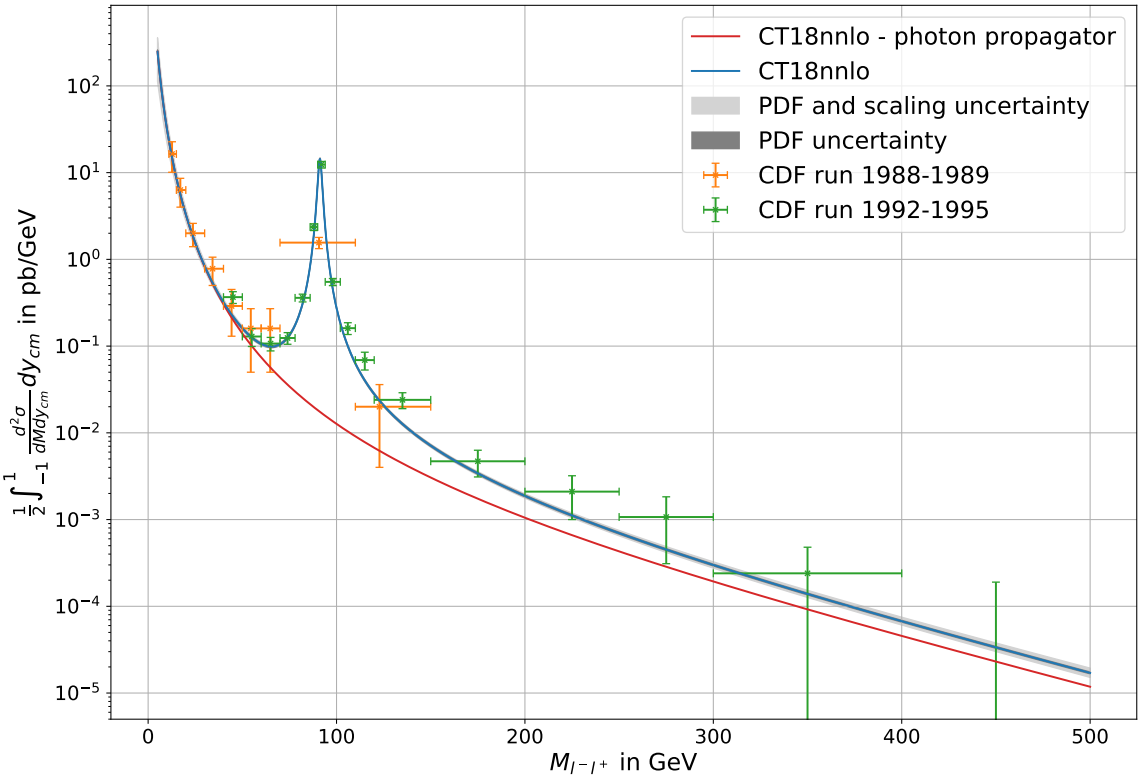

Figure 6: Shown is the experimental data from [11] and [12] and the calculated prediction with CT18nnlo for the full hadronic cross section and only for the photon propagator. For the latter one, only the values are shown without uncertainties. Note that the y-axis is scaled logarithmic.

directly see that there has to be another propagator. Since the Drell-Yan process shows these aberrations well, it is one of the processes that proves the existence of the Z-boson. Furthermore, one may see the areas in which the Z-boson and in which the photon is the main propagator. As in the previous section, the course confirms that the photon propagator dominates in low energy areas, until the Z-boson peak. Now having a closer look again at the mixing term in Eq. 2.85, it is obvious that it becomes negative once the invariant mass of the Z-boson is passed. Knowing this, we spot a slightly steeper decreasing than increasing slope of the peak, which therefore is one relict of the mixed term.

3.3.2. W-Boson

Since both leptons in the final state of the previous process carry charge, they interact with electromagnetic fields and therefore both their momenta may be detected. Thus, the experimental examination of the invariant lepton mass $M_{ll}^2 = (k_1 + k_2)^2$ is straightforward when neglecting technical issues. Hence, the measurement of the Z-boson mass, for example, with the Drell-Yan process, is not that complicated. Considering the charged $W^{\pm}$-bosons, one of the final leptons has to be a neutrino, which cannot be detected directly but only via their reactions like the inverse β-decay. Thus, the experimental determination of the

W-boson mass needs another approach, which we will describe briefly based on [14].

We therefore take the Drell-Yan production with the subprocess $q\overline{q} \to W^+ \to e^+\nu_e$ into consideration. We now define the polar angle θ^* in the rest frame of the W-boson in the same way as in Fig. 2, so as the angle between the collision axis and the outgoing positron. Since the boson has no transverse momentum in lowest order and we neglect the lepton masses, the momentum of the positron may be split into a transverse and longitudinal momentum. This is visualized by the triangle:

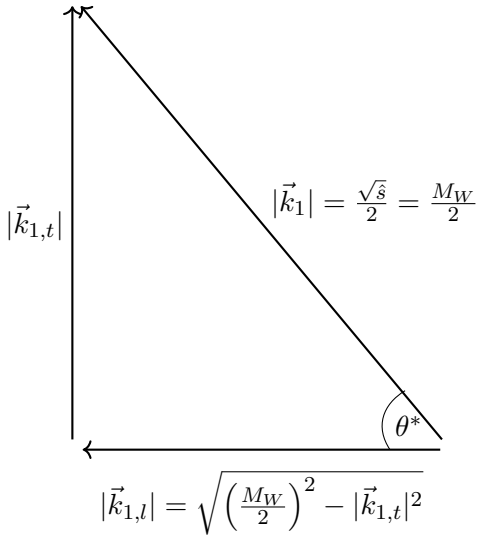

which yields the relation

$$\cos\theta^* = \frac{|\vec{k}_{1,l}|}{|\vec{k}_1|} = \sqrt{1 - \frac{4|\vec{k}_{1,t}|}{M_W^2}}. \tag{3.26}$$

Since we do not know the rest frame of the W-boson, we do not know the angle θ^* either. Nevertheless it is possible to measure the transverse momentum distribution of the positron, which we can now express as

$$\frac{\mathrm{d}\sigma}{\mathrm{d}|\vec{k}_{1,t}|} = -\frac{4|\vec{k}_{1,t}|}{M_W} \frac{1}{\sqrt{1 - \frac{4|\vec{k}_{1,t}|}{M_W^2}}} \frac{\mathrm{d}\sigma}{\mathrm{d}\cos\theta^*}. \tag{3.27}$$

Only because of higher order effects, this does not blow up for $|\vec{k_T}| = M_W/2$. Instead, the derived singularity in leading order shows up as a so called Jacobian peak. So one way to get the W-boson mass is to measure the location of this peak in the cross section. This peak turns out to be smeared out because of the finite width and a non zero transverse momentum of the W-boson. A further approach, which is less sensitive to higher order effects is to measure the transverse mass distribution. For more information one may read [14].

4. Beyond Standard Model

Not only since the discovery of the Higgs boson at the Large Hadron Collider (LHC), BSM theories have high priorities in both theoretical and experimental physicists search for new physics. In this section we want to take a look at the SSM which is a theory that extends the SM. After stating the basic idea of the SSM, we will have a look at the influence of this theory on the already calculated Drell-Yan lepton pair production.

4.1. Sequential Standard Model

In the past the SM predictions succeeded on many occasions and describe the experimental measured data well. Nevertheless, it is widely believed to be incomplete and many beyond SM theories arise which, among other things, suggest further gauge bosons. These new resonances have properties similar to the already known Z- and W-bosons and therefore get the universal names Z'- and W'-bosons. These massive, neutral and charged particles should decay into fermion pairs like their SM equivalent and therefore be detectable in the Drell-Yan lepton pair production[15].

When deriving such heavy resonances, one gets a Lagrangian with a set of free parameters, like the couplings or the mass. In the SSM this freedom is restricted in the most practical way, the new gauge bosons get the same properties as their SM equivalent with just different masses and widths. In the past years, these bosons were searched for in high energy collisions at the Fermilab and LHC. Some of the most recent experimental publications regarding this topic are measurements of lepton pair productions in proton-proton collisions at a centre-of-mass energy of 13 TeV at the ATLAS[16] and CMS[17] detector at the LHC. Neither one could find any derivation from the SM predictions and therefore the lower limit for heavy Z'-boson like suggested in the SSM is set to $M_{Z'} > 5.15\,\text{TeV}$[17].

4.2. Analysis of the Drell-Yan Process in the SSM

In the following step, we want to look at how the Drell-Yan cross section changes if there is a Z'-boson. Especially the interfering of the two bosons will be a central aspect of the discussion. Since nothing like this is found yet, this is just a theoretical model and we may just set the mass to $M_{Z'} = 5\,\text{TeV}$. So it is in the highest area, which may be examined by proton-proton collsions at $\sqrt{S} = 14\,\text{TeV}$ at the LHC when starting the third run in 2022.

We start this discussion by calculating the leftover parts of the partonic and hardonic cross section. It will be practical to go for the same differential cross section as already used in section 3.3. Note that we now consider proton-proton collisions. After visualizing this cross section, we will discuss some new aspects of the SSM Drell-Yan process.

4.2.1. Calculation of the Partonic and Hadronic Cross Section

Taking the SSM Z'-boson into account, we have to adapt the invariant amplitude from Eq. 2.8 to get the right Drell-Yan cross section for an uncharged propagator. Thus, some further terms arise

$$|\mathfrak{M}^2| = |\mathfrak{M}_\gamma^2| + |\mathfrak{M}_Z^2| + |\mathfrak{M}_{Z'}^2| + 2\,\mathrm{Re}\Big\{\mathfrak{M}_\gamma \mathfrak{M}_Z^\dagger\Big\} + 2\,\mathrm{Re}\Big\{\mathfrak{M}_\gamma \mathfrak{M}_{Z'}^\dagger\Big\} + 2\,\mathrm{Re}\Big\{\mathfrak{M}_Z \mathfrak{M}_{Z'}^\dagger\Big\} \quad (4.1)$$

because of the invariant amplitude assigned to the Z' propagator $\mathfrak{M}_{Z'}$. Since the vector bosons Z and Z' only differ in their mass and width, the terms $|\mathfrak{M}_{Z'}^2|$ and $2\,\mathrm{Re}\Big\{\mathfrak{M}_\gamma \mathfrak{M}_{Z'}^\dagger\Big\}$ may be taken from Eq. 2.58 and Eq. 2.74 respectively. Normally we had to calculate the last term $2\,\mathrm{Re}\{\mathfrak{M}_Z \mathfrak{M}_{Z'}\}$ from scratch now, as there is no equivalent in the previous sections. But luckily the computations for $|\mathfrak{M}_Z^2|$ where made in a more general way, so now we can continue from the already spin and color averaged term in Eq. 2.57:

$$\begin{aligned}\overline{\mathfrak{M}_Z \mathfrak{M}_{Z'}^\dagger} = \frac{1}{N}\frac{g^4}{4\cos^4\theta_W}\frac{1}{\left[(\hat{s}-M_Z^2)+iM_Z\Gamma_Z\right]\left[(\hat{s}-M_{Z'}^2)-iM_{Z'}\Gamma_{Z'}\right]} \\ \left\{\left((c_V^q)^2+(c_A^q)^2\right)\left(\left(c_V^l\right)^2+\left(c_A^l\right)^2\right)\frac{\hat{s}^2}{4}(1+\cos^2\theta^*)+2c_V^q c_A^q c_V^l c_A^l \hat{s}^2\cos\theta^*\right\}.\end{aligned} \quad (4.2)$$

In the next step, we have to derive the real part of this term. Since only the fraction with the Z and Z' masses and widths contains something imaginary, we can concentrate on this:

$$\mathrm{Re}\left\{\frac{1}{\left[(\hat{s}-M_Z^2)+iM_Z\Gamma_Z\right]\left[(\hat{s}-M_{Z'}^2)-iM_{Z'}\Gamma_{Z'}\right]}\right\} \quad (4.3)$$

$$= \frac{(\hat{s}-M_Z^2)(\hat{s}-M_{Z'}^2)+M_Z M_{Z'}\Gamma_Z\Gamma_{Z'}}{\left[(\hat{s}-M_Z^2)(\hat{s}-M_{Z'}^2)+M_Z M_{Z'}\Gamma_Z\Gamma_{Z'}\right]^2+\left[(\hat{s}-M_{Z'}^2)M_Z\Gamma_Z-(\hat{s}-M_Z^2)M_{Z'}\Gamma_{Z'}\right]^2} \quad (4.4)$$

$$= \frac{(\hat{s}-M_Z^2)(\hat{s}-M_{Z'}^2)+M_Z M_{Z'}\Gamma_Z\Gamma_{Z'}}{\left[M_Z^2(\Gamma_Z^2-2\hat{s})+M_Z^4+\hat{s}^2\right]\left[M_{Z'}^2(\Gamma_{Z'}^2-2\hat{s})+M_{Z'}^4+\hat{s}^2\right]}. \quad (4.5)$$

Now we got everything to derive the partonic cross section with Eq. 2.81 for the Drell-Yan process with uncharged propagators. Besides Eq. 2.83, Eq. 2.84 and Eq. 2.85 we obtain

$$\hat{\sigma}_{Z'} = \frac{1}{N}\frac{g^4}{192\pi}\frac{1}{\cos^4\theta_W}\frac{\hat{s}}{(\hat{s}-M_{Z'}^2)^2+M_{Z'}^2\Gamma_{Z'}^2}\left((c_V^q)^2+(c_A^q)^2\right)\left(\left(c_V^l\right)^2+\left(c_A^l\right)^2\right) \quad (4.6)$$

$$\hat{\sigma}_{\gamma/Z'} = \frac{1}{N}\frac{g^2\alpha e_q}{6\cos^2\theta_W}\frac{\hat{s}-M_{Z'}^2}{(\hat{s}-M_{Z'}^2)^2+M_{Z'}^2\Gamma_{Z'}^2}c_V^q c_V^l. \quad (4.7)$$

$$\begin{aligned}\hat{\sigma}_{Z/Z'} = \frac{g^4\hat{s}}{96N\pi\cos^4\theta_W}\frac{(\hat{s}-M_Z^2)(\hat{s}-M_{Z'}^2)+M_Z M_{Z'}\Gamma_Z\Gamma_{Z'}}{\left[M_Z^2(\Gamma_Z^2-2\hat{s})+M_Z^4+\hat{s}^2\right]\left[M_{Z'}^2(\Gamma_{Z'}^2-2\hat{s})+M_{Z'}^4+\hat{s}^2\right]} \\ \left((c_V^q)^2+(c_A^q)^2\right)\left(\left(c_V^l\right)^2+\left(c_A^l\right)^2\right).\end{aligned} \quad (4.8)$$

Since we want to get a comparable result, we derive the same differential cross section for proton-proton collisions as before with Eq. 3.16. Note that we also have to switch the PDFs to gain the right parton luminosity factor in Eq. 3.17 so they both refer to protons. We just need to plug in the additional partonic cross sections, which will not be done explicitly as it is quite trivial and add them to the already existing ones.

4.2.2. Modeling of the Cross Section

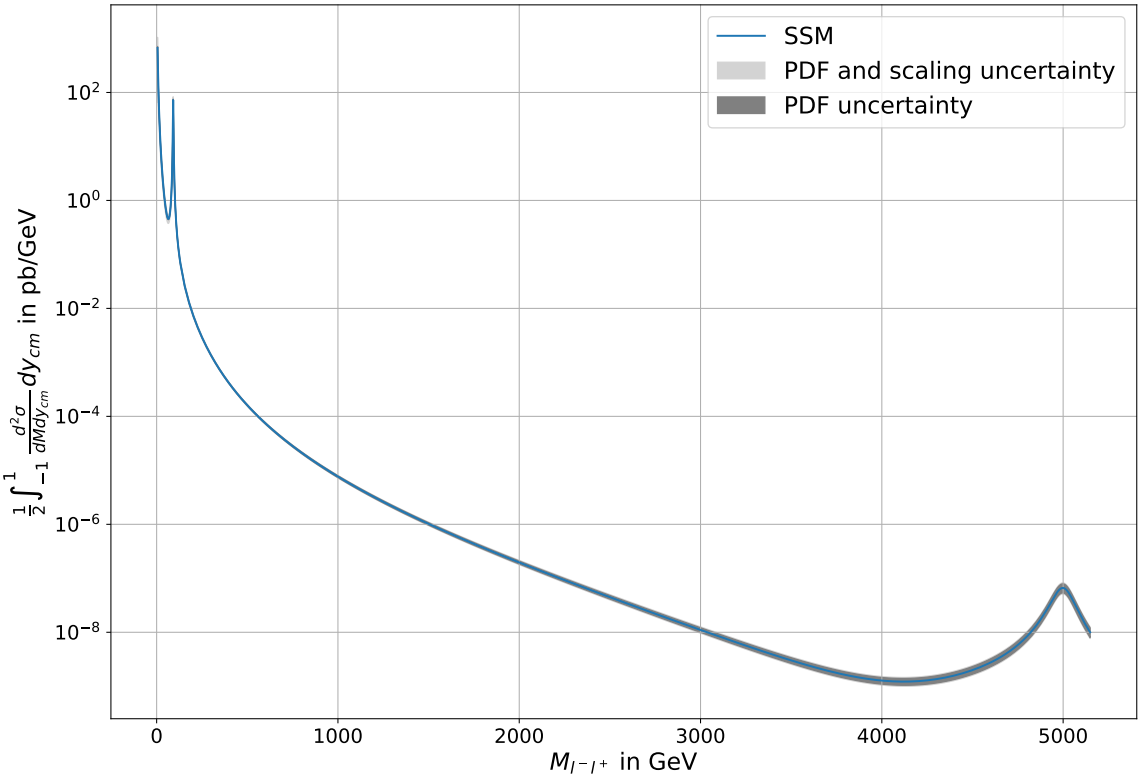

Figure 7: Shown is the differential SSM cross section for proton-proton collisions calculated with the CT18nnlo PDF set.

The SSM cross section is visualized in Fig. 7 with the assigned PDF uncertainties. For these calculations, we used the width $\Gamma_{Z'} = M_{Z'}\Gamma_Z/M_Z \approx 0,027 M_{Z'}$. Thus, the width yields the same fraction of the mass for both bosons. This is, of course, only an assumption that cannot be justified. The Breit-Wigner peaks of both bosons may easily be identified.

A further boson in the cross section cannot be looked at individually, since there are interference terms with the other already existing propagators. In our case, especially the interference of the two bosons lead to significant changes of the peaks. To check this, we will plot the cross section again and compare the predictions for the pure SM, the full SSM and the SSM without the boson interference term. Latter will only be referred to as the interference term. Since the differences are rather small, we only examine the optimum values.

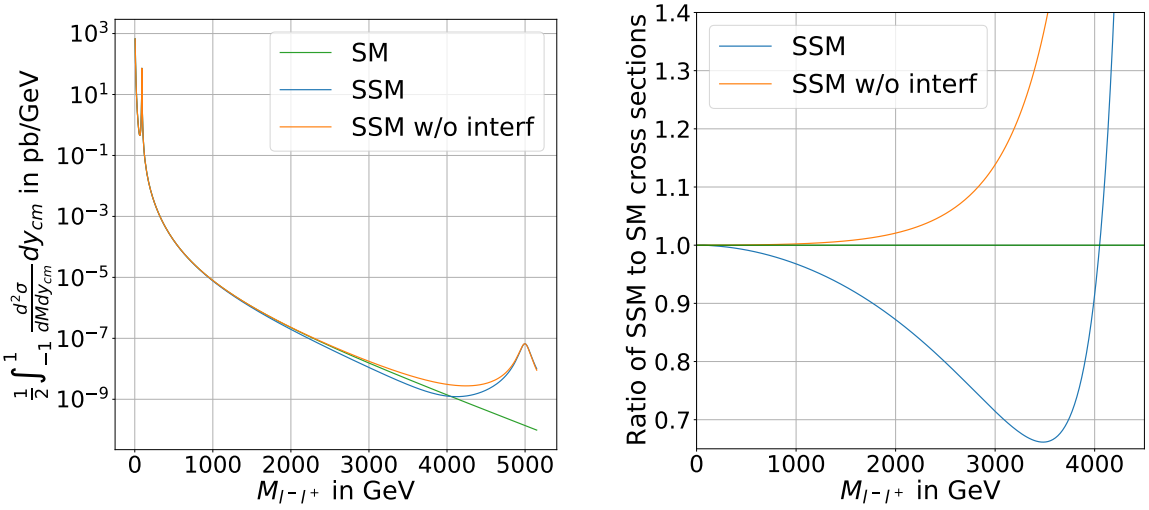

(a) (b)

Figure 8: Shown are the model computations for proton-proton collisions at $\sqrt{S} = 14\,\text{TeV}$ with the CT18nnlo PDF set. In (a) the cross section courses for the three models calculations, pure SM, full SSM and SSM without the interference term are given. In (b) the SSM calculations are shown as the ratio of the SM.

Fig. 8 compares these three model predictions. Conspicuous is the splitting in the intermediate invariant mass range. While the SM prediction decreases as we would have guessed, the SSM starts to increase, building up the Breit-Wigner peak. Looking at the ratios, it is clear to see that the full SSM cross section takes a lower course before rising again, so the interference term lessens the cross section. Of course, there is a slight aberration of these models over the full course. So for exact measurements, the impact of the Z' should be seen around the Z-boson peak as well. Since the abberations are small in this area, for example the SM and SSM calculations are only isolated by $1.3 \cdot 10^{-18}$b at $M_{l^-l^+} = 100\,\text{GeV}$, which is fully covered by the uncertainties, so it is impossible to actually measure this.

Since the Z' resonance was never measured, its width is unknown as well. The impact of different widths in the theoretical modeling is shown in Fig. 9 for four different widths, characterized by their percentage of the assumed Z'-mass. The obvious observation is, of course, the changing height and width of the Z'-peak. Apart from that, the modelings take slightly different courses. So higher cross sections occur for bigger widths except in the direct surrounding area of the Z'-peak. With the help of the zoom in window, one gets an impression on how small the splitting is. Thus, it is not possible to measure the width of a hypothetical Z'-resonance without measuring the peak itself.

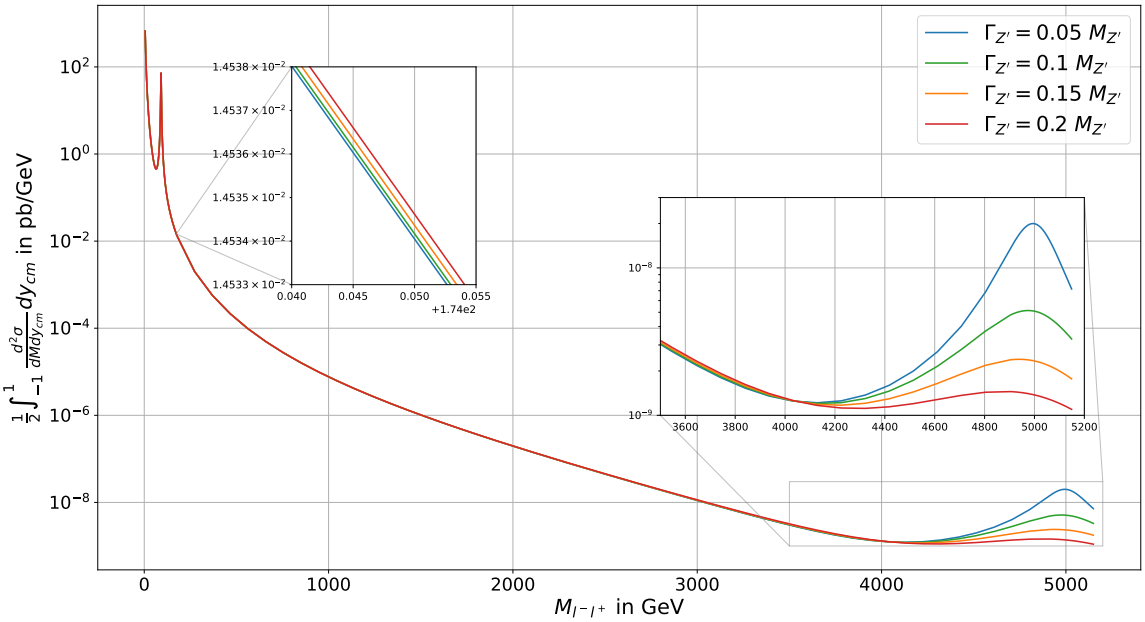

Figure 9: Shown are the model computations for a Z'-boson with different widths. They are given as percentages of its mass, so 5 %, 10 %, 15 % and 20 % respectively.

5. Conclusion

Within this thesis we derived the cross section for dimuon Drell-Yan production via a step-by-step calculation for the assigned subprocess $q\bar{q} \to \gamma/Z^0 \to l^+l^-$ at leading order. Thereby we learned how to handle basic QED processes with the help of Feynman diagrams and rules. While performing the transition from the underlying to the parenting process, we also got in touch with PDFs, which we examined even further before numerically evaluating different cross sections. Especially on the basis of the CT18nnlo PDF set, different properties like their completeness or the change with the scaling energy was discussed.

After covering those general aspects, the numerical evaluation exhibited the scaling behaviour of the Drell-Yan process when only regarding the photon propagator, which is justified in low energy areas far away from the Z-boson mass. Beseides to a good agreement with the theoretical prediction, the experimental data showed peaks which we assigned to different charmonium and bottonium resonances. In higher energy regions, one has to take the Z-boson propagator into account, which yields the characteristic Breit-Wigner peak. Again, despite our only first order calculations, the theoretical prediction were in good agreement with the data of proton-proton collisions. Furthermore, we could divide the cross section into areas mainly affected by the photon or the Z-boson propagator.

In the last section, we examined the effect of a heavier SSM like Z'-boson to the already known cross section. Since no such boson was found yet, the modeling only yields an idea of how it could be. We noticed that such a heavy boson would already change the cross section in energy areas, which are widely explored but in such a minimal way that it is not detectable. Moreover, we also got an insight into the influence of the interference term, which lessens the cross section. Different widths of the Z'-peak also yield a varying course, apart from the obvious change in the peak. Higher width cross sections run at a lower course, if not in the surrounding of the peak. Those differences are again too small to be detectable.

In summary one may say, that the Drell-Yan process is used in many fields of particle physics and its treatment offers a good access to basic collider physics. Of course the examination is extensible for example one could calculate to higher orders to get a deeper insight, consider the explicit calculation of the W-boson, retrace the derivation of PDFs or have a look on more complicated but therefore more probable BSM theories than the SSM. For now it is important to stay curious and await new findings in high energy particle collisions.

Appendix A

In this appendix, we want to give a general overview of some relations used in this thesis. First, we give the applied Feynman rules and afterwards some central aspects of gamma matrices. If not stated differently, all information are based on [2].

A.1 Feynman Rules

To evaluate the invariant amplitude $\mathfrak{M}$ of a particle process, the easiest way is to use the Feynman rules. They connect mathematical expressions with the related Feynman diagram, which is a representation of a particle process with commonly a horizontal time and a vertical room axis. Here, we will only give a brief overview of the rules used in this thesis, by specifying the expressions for the external and internal lines, as well as the vertices. To distinguish, for example, incoming from outgoing particles, all vertices are explicitly indicated with a point when only elements of a diagram are shown.

Since we only operate with quarks and leptons, the rules for external lines only have to cover fermions f and antifermions $\overline{f}$. They are assigned to the spinors $u/\overline{u}$ and $v/\overline{v}$ depending if they are incoming or outgoing. The associated lines are

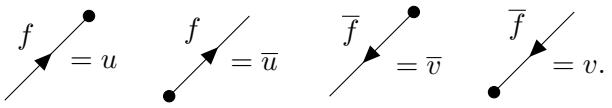

The internal lines differ between the propagators. Below, the expressions for the photon, the Z- and W-boson are given, where M and Γ denote the mass and the width of associated the gauge bosons.

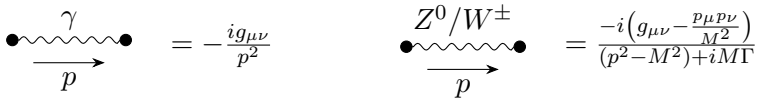

Originally, all calculation where intended to be at tree level, which means lowest order in perturbation theory. The only exception occurs in the denominator of the gauge-boson propagator. At tree level one would only get the term $(p^2 - M^2)$ which would yield a delta-peak when $p^2 = M^2$, which wouldn't be accurate. Therefore, we consider higher orders and derive the Breit-Wigner resonance as it is shown. Since the influence of this is higher than all the higher order terms of the other Feynman diagram parts, one may still neglect them.

At last the vertex factors for the different propagators are given below. Note that the four-momentum is conserved at vertices. Q_f gives the charge of the fermions in units of the elementary charge e. The Weinberg angle θ_W is the weak mixing angle of the electroweak

interaction, where Photon and Z-boson are just different combinations of the B^0- and the W^0-boson. g is the associated coupling constant working for the Z- and W-bosons.

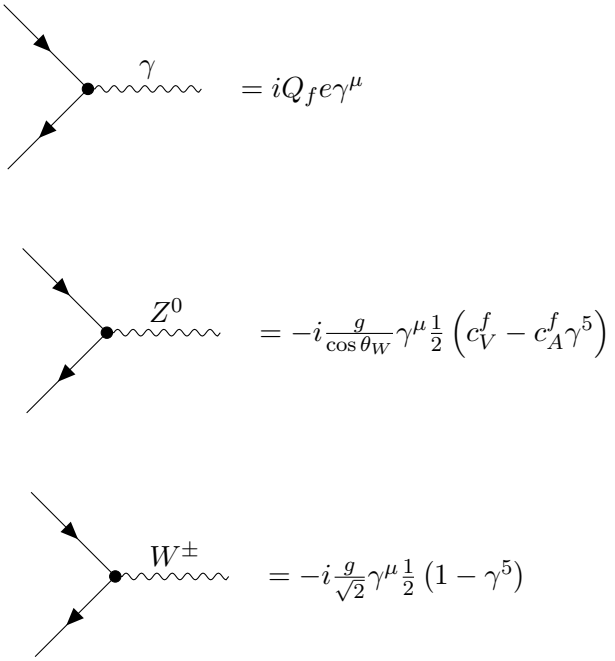

The last, not yet discussed factor is the term in the brackets. Seeing it in the full context of the invariant amplitude, it gets multiplied with a gamma matrix from the left and a spinor from each side, yielding a vector and an axial vector for c_V^f and $c_A^f\gamma^5$ respectively. To conserve parity, an interaction has to be of pure vector or axial vector type. The former takes place, for example, in electromagnetic interaction. So the term in the brackets shows that the Z-boson couples to left- and right-handed fermions with different strength. The W-boson vector and axial vector part has the same size but a different sign, which is sometimes called a $(V-A)$-coupling. It follows that the W-boson only couples to left-handed fermions and right-handed antifermions[8].

One may get the final invariant amplitude $-i\mathfrak{M}$ for a process by multiplying the mathematical expressions of the parts in the right order. For the external lines and vertices the proper sequence is overlined spinor, vertex and spinor, which yields a scalar. This expression for incoming and outgoing external lines needs to be multiplied by each other and by the likewise scalar propagator factor. If there are multiple equivalent Feynman-diagrams for one process, the invariant amplitudes add up to the full one.

A.2 Gamma Matrices, Trace Relations and More

Since there are a lot of relations regarding, for example, gamma matrices and their traces, it would go beyond the scope of this thesis to give a full summary. Therefore, we will only give some relations, which are especially emphasized in the text. Thereby, we renounce on any derivation, which may be looked up, for example in [2] if interested.

A quite important connection between the spinors yields the completeness relation

$$\sum_s u^{(s)}(p)\ \overline{u}^{(s)}(p) = \not{p} + m \qquad\qquad \sum_s v^{(s)}(p)\ \overline{v}^{(s)}(p) = \not{p} - m \tag{A.1}$$

with the Feynman slash notation $\not{A} = \gamma^\mu A_\mu$.

Using the indices $\mu, \nu \in \{0, 1, 2, 3\}$ some of the central gamma matrix relations are:

$$\gamma^{\mu\dagger} = \gamma^0\gamma^\mu\gamma^0 \qquad (\gamma^o)^2 = \mathbb{1}_{4\times4} \qquad \gamma^\mu\gamma^\nu + \gamma^\nu\gamma^\mu = 2g^{\mu\nu} \tag{A.2}$$

$$\gamma^5 = i\gamma^0\gamma^1\gamma^2\gamma^3 \qquad \left(\gamma^5\right)^2 = \mathbb{1}_{4\times4} \qquad \gamma^5\gamma^\mu + \gamma^\mu\gamma^5 = 0. \tag{A.3}$$

One may also derive a set of trace relations with the gamma matrices. In this thesis, we used:

$$\mathrm{Tr}\{\gamma^\mu\gamma^\nu\gamma^\rho\gamma^\sigma\} = 4\left(g^{\mu\nu}g^{\rho\sigma} - g^{\mu\rho}g^{\nu\sigma} + g^{\mu\sigma}g^{\nu\rho}\right) \tag{A.4}$$

$$\mathrm{Tr}\{\gamma_\mu\gamma_\nu\gamma_\rho\gamma_\sigma\} = 4\left(g_{\mu\nu}g_{\rho\sigma} - g_{\mu\rho}g_{\nu\sigma} + g_{\mu\sigma}g_{\nu\rho}\right) \tag{A.5}$$

$$\mathrm{Tr}\left\{\gamma^\alpha\gamma^\beta\gamma^\delta\gamma^\lambda\gamma^5\right\} = -4i\epsilon^{\alpha\beta\delta\lambda}. \tag{A.6}$$

To handle the totally antisymmetric tensor right, we use the connections given in [18]:

$$\epsilon^{0123} = -\epsilon_{0123} = 1 \tag{A.7}$$

$$\epsilon_{\alpha\beta\mu\nu}\epsilon^{\alpha\beta\lambda\rho} = \epsilon_{\mu\nu\alpha\beta}\epsilon^{\lambda\rho\alpha\beta} = -2\left(\delta^\lambda_\mu\delta^\rho_\nu - \delta^\rho_\mu\delta^\lambda_\nu\right) \tag{A.8}$$

$$\begin{aligned}\epsilon_{\beta\nu\alpha\mu}\epsilon^{\beta\rho\sigma\lambda} = {} & \delta^\lambda_\alpha\delta^\rho_\nu\delta^\sigma_\mu + \delta^\rho_\alpha\delta^\sigma_\nu\delta^\lambda_\mu + \delta^\lambda_\nu\delta^\rho_\mu\delta^\sigma_\alpha \\ & - \delta^\lambda_\mu\delta^\rho_\nu\delta^\sigma_\alpha - \delta^\lambda_\nu\delta^\rho_\alpha\delta^\sigma_\mu - \delta^\rho_\mu\delta^\sigma_\nu\delta^\lambda_\alpha\end{aligned} \tag{A.9}$$

$$g^{\eta\nu}g_{\nu\rho} = g_{\rho\nu}g^{\nu\eta} = \delta^\eta_\rho. \tag{A.10}$$

Using this one may show:

$$\epsilon_\beta{}^{\tau\eta\theta}\epsilon^\beta{}_\tau{}^{\sigma\lambda} = g^{\tau\nu}g^{\eta\alpha}g^{\theta\mu}g_{\tau\rho}\,\epsilon_{\beta\nu\alpha\mu}\epsilon^{\beta\rho\sigma\lambda} \tag{A.11}$$

$$= 2\left(g_{\lambda\eta}g_{\theta\sigma} - g_{\theta\lambda}g_{\eta\sigma}\right). \tag{A.12}$$

Bibliography

[1] S. D. Drell and T. Yan. "Massive Lepton-Pair Production in Hadron-Hadron Collisions at High Energies". In: *Phys. Rev. Lett.* 25 (5 1970), pp. 316–320. DOI: 10.1103/PhysRevLett.25.316.

[2] F. Halzen and A. D. Martin. *Quarks and Leptons: An Introductory Course in Modern Particle Physics*. John Wiley & Sons, 1984. ISBN: 0471887412.

[3] T. Han. "Collider Phenomenology: Basic Knowledge and Techniques". In: *Theoretical Advanced Study Institute in Elementary Particle Physics: Physics in D≥4*. 2005. DOI: 10.1142/9789812773579_0008. arXiv: hep-ph/0508097.

[4] Tie-Jiun Hou et al. "New CTEQ global analysis of quantum chromodynamics with high-precision data from the LHC". In: *Phys. Rev. D* 103.1 (2021), p. 014013. DOI: 10.1103/PhysRevD.103.014013. arXiv: 1912.10053 [hep-ph].

[5] Andy Buckley et al. "LHAPDF6: parton density access in the LHC precision era". In: *The European Physical Journal C* 75.3 (Mar. 2015). ISSN: 1434-6052. DOI: 10.1140/epjc/s10052-015-3318-8. URL: http://dx.doi.org/10.1140/epjc/s10052-015-3318-8.

[6] Jacob J. Ethier and Emanuele R. Nocera. "Parton Distributions in Nucleons and Nuclei". In: *Annual Review of Nuclear and Particle Science* 70.1 (Oct. 2020), pp. 43–76. ISSN: 1545-4134. DOI: 10.1146/annurev-nucl-011720-042725. URL: http://dx.doi.org/10.1146/annurev-nucl-011720-042725.

[7] K. Kovarík et al. "nCTEQ15: Global analysis of nuclear parton distributions with uncertainties in the CTEQ framework". In: *Phys. Rev. D* 93 (8 Apr. 2016), p. 085037. DOI: 10.1103/PhysRevD.93.085037. URL: https://link.aps.org/doi/10.1103/PhysRevD.93.085037.

[8] B. Povh, K. Rith, et al. *Particles and Nuclei. An Introduction to the Physical Concepts*. Springer-Verlag GmbH, 2015. ISBN: 9783662463208.

[9] D. M. Alde et al. "Nuclear dependence of dimuon production at 800 GeV". In: *Phys. Rev. Lett.* 64 (21 May 1990), pp. 2479–2482. DOI: 10.1103/PhysRevLett.64.2479. URL: https://link.aps.org/doi/10.1103/PhysRevLett.64.2479.

[10] Particle Data Group. *The Review of Particle Physics (2021)*. 2021. URL: https://pdg.lbl.gov/ (visited on 08/20/2021).

[11] F. Abe et al. "Measurement of Drell-Yan electron and muon pair differential cross sections in $\overline{p}p$ collisions at $\sqrt{s} = 1.8$ TeV". In: *Phys. Rev. D* 49 (1 Jan. 1994), R1–R6. DOI: 10.1103/PhysRevD.49.R1. URL: https://link.aps.org/doi/10.1103/PhysRevD.49.R1.

[12] F. Abe et al. "Measurement of Z^0 and Drell-Yan production cross sections using dimuons in $\overline{p}p$ collisions at $\sqrt{s} = 1.8$TeV". In: *Phys. Rev. D* 59 (5 Jan. 1999), p. 052002. DOI: 10.1103/PhysRevD.59.052002. URL: https://link.aps.org/doi/10.1103/PhysRevD.59.052002.

[13] R. K. Ellis, W.J. Stirling, and B.R. Webber. *QCD and Collider Physics*. The press syndicate of the University of Cambridge, 1996. ISBN: 0521581893.

[14] Matthew D. Schwartz. *TASI Lectures on Collider Physics*. 2017. arXiv: 1709.04533 [hep-ph].

[15] Tomas Jezo. "Z' and W' gauge bosons in SU(2)xSU(2)xU(1) models : Collider phenomenology at LO and NLO QCD". PhD thesis. LPSC, Grenoble, 2013.

[16] G. Aad et al. "Search for high-mass dilepton resonances using 139 fb1 of pp collision data collected at s=13 TeV with the ATLAS detector". In: *Physics Letters B* 796 (Sept. 2019), pp. 68–87. ISSN: 0370-2693. DOI: 10.1016/j.physletb.2019.07.016. URL: http://dx.doi.org/10.1016/j.physletb.2019.07.016.

[17] CMS Collaboration. "Search for resonant and nonresonant new phenomena in high-mass dilepton final states at $\sqrt{s} = 13$ TeV". In: *JHEP* 2107 (Mar. 2021). Replaced with the published version. Added the journal reference and the DOI. All the figures and tables, including additional supplementary figures, can be found at http://cms-results.web.cern.ch/cms-results/public-results/publications/EXO-19-019 (CMS Public Pages), 208. 58 p. DOI: 10.1007/JHEP07(2021)208. arXiv: 2103.02708. URL: https://cds.cern.ch/record/2753579.

[18] V. I. Borodulin, R. N. Rogalyov, and S. R. Slabospitskii. *CORE 3.1 (COmpendium of RElations, Version 3.1)*. 2017. arXiv: 1702.08246 [hep-ph].

Declaration of Academic Integrity

I hereby confirm that this thesis on *Drell-Yan Process in the Standard Model and Beyond* is solely my own work and that I have used no sources or aids other than the ones stated. All passages in my thesis for which other sources, including electronic media, have been used, be it direct quotes or content references, have been acknowledged as such and the sources cited.

Münster, September 6, 2021 

(signature of student)

I agree to have my thesis checked in order to rule out potential similarities with other works and to have my thesis stored in a database for this purpose.

Münster, September 6, 2021 

(signature of student)